REVIEW

Chinese Journal of Structural Chemistry

Lithium Ion Conduction in Covalent Organic Frameworks

Sijia Liu[1,2], Minghao Liu[2], Qing Xu[2,3]* and Gaofeng Zeng[2,3]*

[1]*School of Physical Science and Technology, ShanghaiTech University, Shanghai 201210, China*

[2]*CAS Key Laboratory of Low-carbon Conversion Science and Engineering, Shanghai Advanced Research Institute, Chinese Academy of Science, Shanghai 201210, China*

[3]*School of Chemical Engineering, University of Chinese Academy of Sciences, Beijing 100049, China*

ABSTRACT Ion conduction plays key roles in electrochemical systems, including fuel cells, lithium ion batteries, and metal-air batteries. Covalent organic frameworks (COFs), as a new class of porous polymers, constructed by pre-designable building blocks, are ideal hosts to accommodate ionic carries for conduction because of their straightforward pore channels, tunable pore size, controllable pore environment, and good chemical and thermal stability. Different from proton conduction, how to achieve high lithium ion conduction is still a challenge as it is difficult to dissociate ionic bonds of the lithium salts. To facilitate the dissociation of lithium salts, COFs with different pores and skeletons are well designed and constructed. This review focuses on emerging developments of lithium ion conduction in COFs, and discusses the structures of these COFs and conductive performance to elucidate the structure-property correlations. Furthermore, we have concluded the remaining challenge and future direction in these COF-based lithium conductive areas. This review provides deeper insight into COFs for ionic conduction.

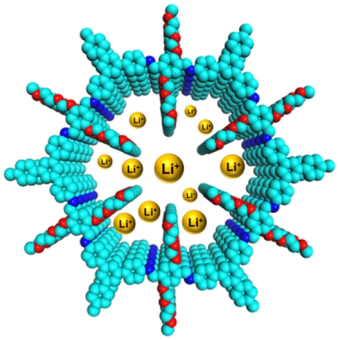

Keywords: covalent organic frameworks, ionic conduction, lithium ion conduction, pore surface engineering, ionic COFs

n INTRODUNTION

Covalent organic frameworks (COFs), as a class of porous polymers, are constructed by organic building blocks via covalent bonds, displaying high chemical and thermal stability.[1-14] The organic building blocks in COFs are linked through reversible reactions, and various linkages are classified into boron-based linkages (B-O), nitrogen-based linkages (C=N, N=N, and C-N), oxyngen-based linkage (O-C), and carbon-based linkages (C=C).[15-20] In addition to various linkages, the geometry of building blocks determines the different pore shapes of one-dimensional channels in COFs, such as hexagonal, tetragonal, rhombic, and trigonal shapes.[21-25] The elegant π skeletons together with porous nature of COFs provide a fundamental basis for structural design. COFs can be designed and synthesized for different applications, including sensors,[26-30] gas storage and separation,[31-35] molecular separation,[36-38] photocalysis,[39-42] drug delivery,[43-45] water harvesting,[46] and catalysts.[47-50] Moreover, COFs have one-dimensional tailor-made channels, which provides fast pathway for ion and molecule transport.[51-56] These controllable channels together with electrochemical active skeletons render COFs to be used in electrochemical energy storage and conversion systems, including lithium-ion batteries,[57-59] sodium-ion batteries,[60-62] potassium-ion batteries,[63-66] lithium-sulfur batteries,[67-70] capacitors,[71] electrocatalysis,[72-74] and metal-air cells.[75]

In lithium-ion batteries, electrolytes play important roles in Li^+ transport between electrodes. Most batteries use organic liquid electrolytes, which causes many problems because they are leaked and combustible.[76,77] And the low work potential of liquid electrolytes limits the practical application. Moreover, the thermal stability is another severe problem. To solve these critical problems, the best method is developing solid electrolytes to replace liquid electrolytes.

The solid electrolytes are classified into inorganic electrolytes and polymer electrolytes.[78-81] Different from inorganic electrolytes, polymer electrolytes displayed many advantages, such as easy fabrication, outstanding chemical stability and flexibility.[82-84] However, their low ionic conductivity, poor mechanical strength and thermal dimensional stability limit the polymer electrolytes in practical application. The characters of polymers cause these bottleneck issues. For example, the high crystallinity of polymers, low melting temperature, and the disordered structure could not provide fast transport pathway as inorganic electrolytes.[85,86] The frameworks of COFs possessed good chemical and thermal stability and the pore environment in 1D channels, which can be accurately tuned, thus allowing COFs for lithium ion conduction.

The integration of well-defined structural ordering, tunable porosity and functionality, and robust thermal and chemical stability in one extended COF structure is hardly achieved by other porous materials. In this review, we focus on recent advances in the application of lithium ion conduction on the structure of COFs materials. Recently, there are many reports about the utilization of COFs in ion conduction. The lithium ion conductivity and conductive mechanism are related to the pores and skeletons of COFs. The conductivity (σ) is defined by $\sigma = c_i \times \mu$, where c_i is the ion concentration and μ is the ion mobility. The ion conduction mechanism was obtained by plotting conductivity versus temperature. When the active energy (E_a) is smaller than 0.4 eV, the mechanism is Grotthuss mechanism, and the mechanism is Vehicle mechanism for ionic conduction with the E_a value over

DOI: 10.14102/j.cnki.0254-5861.2022-0114

0.4 eV. In bare COFs, the high pore volumes of COFs enable to load high concentration of hybrids of lithium ion and electrolytes, which is helpful to achieve high conductivity. However, the resulting electrolytes are quality solid-state Li^+ conductors. In polyelectrolyte COFs, the higher density or longer polyelectrolyte chains in the pores facilities lithium ion mobility and low *Ea*; however, these chains block the pores and cause lower surface areas and lower porosity, which result in low lithium ion contents in the pores. To achieve high σ values, the contents and the length of chains should be previously controlled. In anion COFs, the cationic skeletons can trap the anions of lithium salts, and accelerate Li^+ transport, leading to high lithium ion transfer numbers.

Accordingly, we summarize the current progress of COFs for lithium ion conduction, discuss and elaborate the impact of the pore size, shapes and environments in COFs on conductive performance. Furthermore, we analyze the challenges of COFs for application in ion conduction. We hope our work helps researchers to develop COFs with excellent ion conduction performance in energy storage and conversion systems.

n BARE COFS FOR LITHIUM ION CONDUCTION

The pressure-induced crystallographic preferred orientation for COFs is an attractive feature, which facilitates mass transfer within the aligned cylindrical pores in the COF pellets. In 2016, Fernando J. Uribe-Romo and his co-workers have first used COFs for lithium ion conduction.[87] Five COFs with different linkages (COF-1 (boroxine), TpPa-1COF (β-ketoenamine), CTF-1 (triazine), and tetragonal ZnPc-BBA COF (boronate)) were successfully synthesized to accommodate lithium salts. The powder X-ray diffraction (PXRD) pattern revealed pressure-induced crystallographic preferred orientation for COFs. And the powder samples of COF-5 and Tppa-1 COF (Figure 2) were treated with 1 M $LiClO_4$/THF for 48 h to load 3.77 mol% Li^+ ions. The resulting pallets for COF-5 and Tppa-1 COF exhibited ionic conductivities of 0.26 and 0.15 mS cm^{-1} at room temperature, respectively. The pallets without Li^+ salts showed no Nyquist behavior, suggesting the conductive behavior attributed to the Li^+. Isotropic ^7Li MAS NMR spectrum of Li-treated COF-5 exhibits only a single resonance, revealing that all the lithium ions are confined in the pores rather than on the surface of COF-5. Moreover, by using linear Arrhenius plot, the E_a was evaluated to be 0.037 ± 0.004 eV for COF-5. The low activation energy indicates that the ion conductivity retains over a wide temperature range. The ^7Li static solid-state nuclear magnetic resonance (ssNMR) spectrum of the $LiClO_4$-impregnated COF-5 (powder) was compared to that of $LiClO_4$, finding the relaxation time for $LiClO_4$ in the pores of COF is about 1.91 s, which is 4 orders of magnitude smaller than that of $LiClO_4$ (2426 s). Thus, the 1D channels promote lithium ion conduction.

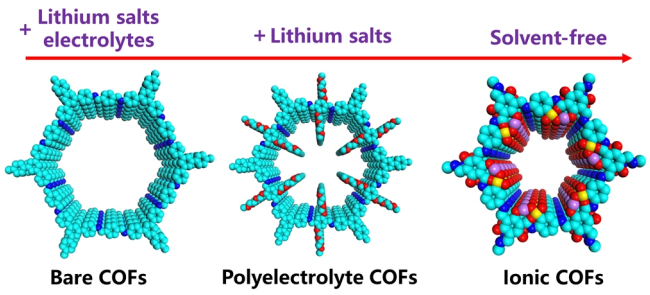

Figure 1. Constructing COFs by using different strategies for lithium ion conduction.

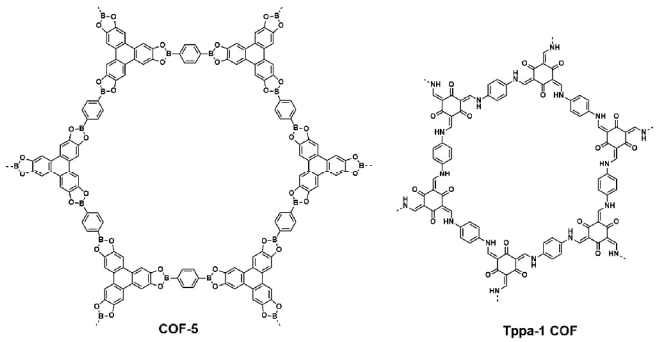

Figure 2. Chemical structures of COF-5 and Tppa-1 COF.

To overcome the difficulty of dissociation of lithium salts, adding electrolytes into the pores together with lithium salts is an effective approach. Low-molecular-weight polyethylene glycol (PEG) possesses much higher chain dynamics and provides a great chance to reach a high ion conduction rate than that of PEO, which has high contents of crystalline regions. Nevertheless, the melting temperature made PEG undergo a phase change from an elastic to viscous state with increasing the working temperature. Encapsulating PEG into the pores of COFs provides a chance to solve the problem. Recently, a COF

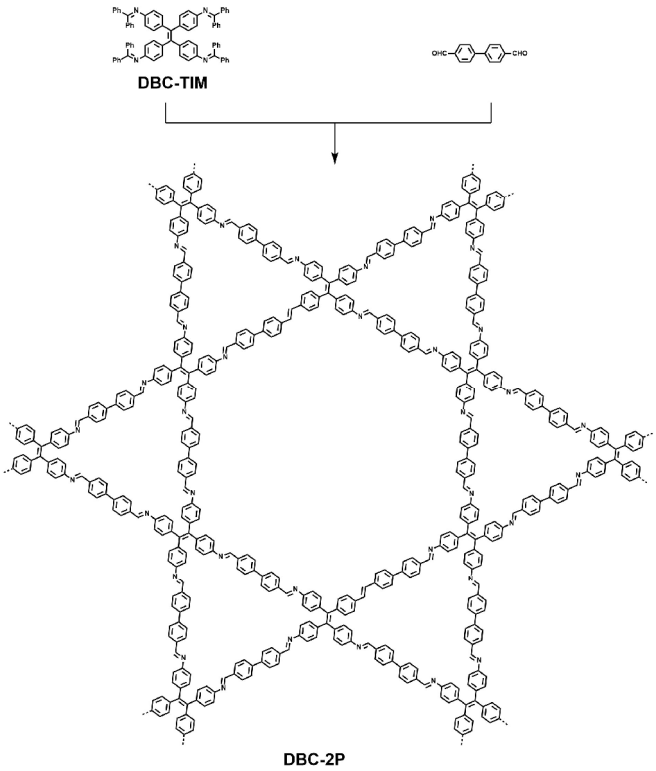

Figure 3. Synthesis of DBC-2P.

DOI: 10.14102/j.cnki.0254-5861.2022-0114

(DBC-2P) has been synthesized from DBC-TIM and 4,4'-biphenyldicarbaldehyde (BPDA) monomers (Figure 3).[88] The DBC-2P has a BET surface area of 1203 m^2 g^{-1}, with a total volume of 0.87 cm^3 g^{-1}. DBC-2P possessed ordered 1D dual-pore nanochannels, with pore sizes of 1.19 and 3.24 nm, respectively, close to the theoretical arithmetic value. DBC-2P exhibited excellent stability both in strong acid and base due to the large conjugated DBC-based knot that reinforces the inter-layer interactions. PEG (M = 1000) with different amounts, as a guest, was then introduced into the pores of DBC-2P, with the composite samples denoted as DBC-2P⊂PEG-X wt%. The transition temperature of confined PEG is positively correlated to the pore size of porous matrices. The endothermic peak for DBC-2P⊂PEG-28% is at -20 °C because of PEG confined in the channels. And with increasing the contents of PEG to 45%, a new peak at 37 °C can be observed, indicating PEG is on the outsides of COFs. DBC-2P⊂PEG-28% displayed a conductivity of 4.50 × 10^{-5} S cm^{-1} at 70 ºC under 98% at room temperature, however, that of DBC-2P⊂PEG-28% is about 2.84 × 10^{-9} S cm^{-1} at the same temperature under anhydrous condition, indicating water capature in pores can promote the ion conduction. The complex of PEG and $LiBF_4$ was then introduced into the pores

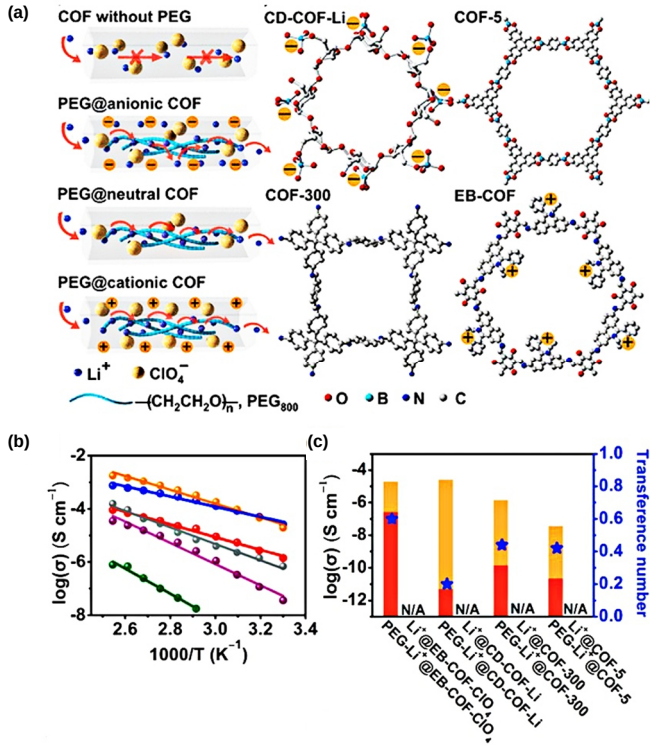

Figure 4. (a) Schematic illustrations of Li^+ transport in COFs (CD-COF, COF-5, COF-300, and EB-COF. (b) Arrhenius plots of PEG-Li^+@COFs (PEG-Li^+@CD-COF-Li (green), PEG-Li^+@EB-COF-ClO_4 (orange), PEG-Li^+@COF-5 (purple), PEG-Li^+@COF-300 (red), and PEG/Li+/EB-COF-ClO_4 (purple). (c) Ion conductivities and T_{Li+} of PEG PEG-Li^+@ COFs and Li^+@COFs at 30 °C, in which the red area indicates the lithium ion conductive attribution and the orange area shows the anion conductive attribution. Reproduced with permission from ref. 89.

(DBC-2P⊂PEG-$LiBF_4$). The ion conductivities were 2.31 × 10^{-3} S cm^{-1} at 70 ºC under 98% RH and 6.16 × 10^{-9} S cm^{-1} under anhydrous condition. The E_a values for DBC-2P⊂PEG-$LiBF_4$ and DBC-2P⊂PEG-28% are 0.09 and 0.20 eV, respectively. To better understand the conductivity from the lithium ion transport, the ^7Li solid-state NMR and ^1H solid-state NMR spectra were conducted. Accordingly, the full width at half maximum of signals decreased with increasing the humidity, which suggested that synergistic effect of H_2O and Li^+ promoted ion conduction. Thus, loading PEG and H_2O promoted lithium ion conduction in channels.

Pore environments of COFs have also greatly influenced the lithium ion conduction. To illustrate the relationship between the lithium ion conduction and pore structures, COFs with different skeletons (anion skeleton (CD-COF), cationic skeleton (EB-COF-ClO_4) and neutral skeleton (COF-5 and COF-300)) have been successfully synthesized. Such COFs were used as a host to load PEG (M = 800) and $LiClO_4$ to obtain PEG-Li^+@COFs for lithium ion conduction (Figure 4).[89] And the mechanical mixture of PEG, $LiClO_4$, and EB-COF-ClO_4 was prepared for control. The DSC analysis for PEG-Li^+@COFs shows no obvious endothermic/exothermic peak in the DSC profile of PEG-Li^+@EB-COF-ClO_4, whereas there is thermal transition at about 30 °C for pure PEG. And PEG/Li^+/EB-COF-ClO_4 exhibits similar thermal behavior with bulk PEG. Thus, PEG and $LiClO_4$ were confined into the pores of PEG-Li^+@EBCOF-ClO_4. The conductive performance was studied from 30 to 120 °C. The ion conductivities of PEG-Li^+@CD-COF-Li, PEG-Li^+@COF-300, PEG-Li^+@COF-5, and PEG-Li^+@EB-COF-ClO_4 are 2.60 × 10^{-5}, 1.40 × 10^{-6}, 3.60 × 10^{-8} and 1.93 × 10^{-5} S cm^{-1} at 30 °C, respectively. And the conductivities of PEG-Li^+@CD-COF-Li, PEG-Li^+@COF-300, PEG-Li^+@COF-5, and PEG-Li^+@EB-COF-ClO_4 are 1.30 × 10^{-4}, 9.11 × 10^{-5}, 3.49 × 10^{-5} and 1.78 × 10^{-3} S cm^{-1} at 120 °C. PEG-Li^+@CD-COF-Li and PEG-Li^+@EB-COF-ClO_4 displayed higher conductivity than PEG-Li^+@COF-300 and PEG-Li^+@COF-5, further proving the interaction between the charged frameworks and lithium salts, which promotes the dissociation of ionic pairs. And the E_a values calculated according to the Arrhenius law are as low as 0.17, 0.20, 0.35, and 0.21 eV for PEG-Li^+@CD-COF-Li, PEG-Li^+@COF-300, PEG-Li^+@COF-5, and PEG-Li^+@EB-COF-ClO_4 correspondingly (Figure 4b). The conductivity for PEG/Li^+/EB-COF-ClO_4 is 7.81 × 10^{-7} S cm^{-1} at 30 ºC, further confirming that PEG in channels favored lithium ion conduction along the channels. The lithium ion transference numbers (T_{Li}^+) for PEG-Li^+@CD-COF-Li, PEG-Li^+@COF-300, PEG-Li^+@COF-5, and PEG-Li^+@EB-COF-ClO_4 are 0.2, 0.44, 0.40 and 0.60 (Figure 4c). The cationic skeleton of EB-COF-ClO_4 can trap the anion and accelerate the Li^+ transport.

The traditional form of COF based electrolytes is solid powder, which greatly limits their practical applications. Thus, fabricating COF based membrane electrolytes is significant. Recently, Zhang and his co-workers have constructed COF membrane via interfacial polymerization reaction, and then incorporated PEG into the pore channel for lithium ion conduction.[90] The prepared COF membrane (COF-M) has maximum nitrogen adsorption of 702.57 cm^3 g^{-1}, with a pore size of 2.5 nm (Figure 5a). The com-

DOI: 10.14102/j.cnki.0254-5861.2022-0114

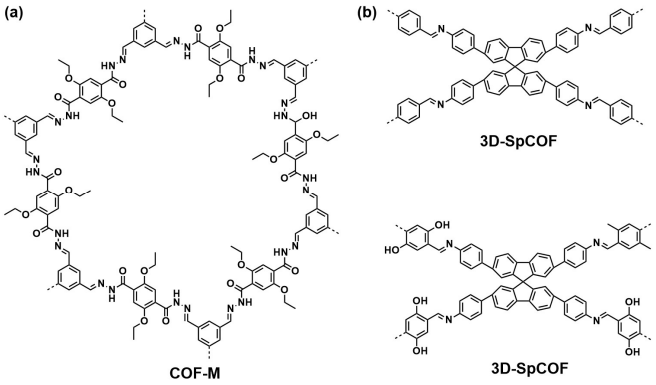

Figure 5. Chemical structures of (a) COF-M, (b) 3D-SpCOF and 3D-SpCOF-OH.

plex of PEG and Li^+ was infiltrated into dry membrane to obtain the PEG-Li^+@COF-M, while mixing the PEG/Li^+ with commercial separator to yield PEG-Li^+@Spe. The chemical sate of Li^+ in PEG-Li^+@COF-M and PEG-Li^+@Spe is different because the COF-M provides 1D channels in nano-scale, while the space in Spe was from micro-space. The ionic conductivities for PEG-Li^+@Spe are 3.4×10^{-8} and 5.0×10^{-6} S cm^{-1} at 20 and 80 ºC, respectively. Notebly, the conductivies for PEG-Li^+@COF-M are 2.2×10^{-5} and 4.0×10^{-4} S cm^{-1} at the same temperature. PEG-Li^+@COF-M has a smaller E_a value of 0.46 eV than PEG-Li^+@Spe (0.51 eV), suggesting its lower Li^+ energy barrier. In addition, PEG-Li^+@ COF-M has excellent long-term stability at 120 ºC for 48 h, with a stable ionic conductivity of 1.9×10^{-3} S cm^{-1}. The battery based on COF-membrane achieved specific discharge capacity of 135.7 mAh g^{-1} after 80 cycles with 97.6% Coulombic efficiency.

In addition to PEG-based additive, plastic crystal (succinonitrile (SN)) is also adopted to facilitate lithium ion transport.[91] 3D COFs (3D-SpCOF and 3D-SpCOF-OH) constructed on spirobifluorene core were synthesized as the host for loading SN and lithium sources (Figure 5b). The free-standing COF pellets were prepared via the cold-pressing method. The mixture of SN and LiTFSI was added on the surface of COF pellets which were fast absorbed into the pores of COFs. The ionic conductivities for 3D-SpCOF-SSE and 3D-SpCOF-OH-SSE are 0.64 and 1.21 mS cm^{-1} at room temperature, respectively, and the higher value for the latter can be attributed to that the OH groups promoted the dissociation of ion pairs. 3D-SpCOF-SSE showed different E_a values of 0.13 and 0.015 eV below and above 50 ºC (the melting temperature for SN). Surprisingly, the the Arrhenius plots of 3D-SpCOF-OH-SSE can be well fitted by Arrhenius and Vogel-Tammann-Fulcher (VTF) models, because the OH group in the skeleton promotes the dissolution of SN. Similar skeletons make 3D-COFs have close values of T_{Li^+} (0.70 for 3D-SpCOF-SSE and 0.64 for 3D-SpCOF-OH-SSE). The theoretical calculation revealed the Li^+ favors along the *x* axial pathway compared to the *y* and *z* axes. The assembling solid-state batteries based on 3D-SpCOF-based SSE displayed stable and reversible cycling performance at room temperature.

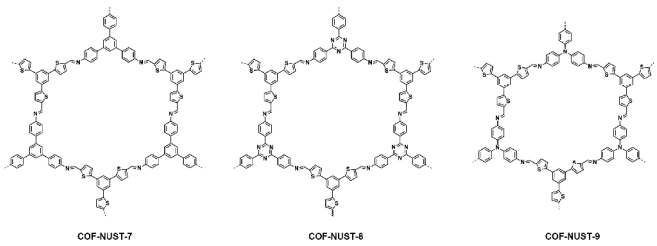

Figure 6. Chemical structures of COF-NUST-7, 8, 9.

Recently, ionic liquids (IL) have been loaded in the COFs for lithium ion conduction. ILs are a class of ionic carriers because of their low volatility, high thermal and electrochemical stability, and excellent ionic conductivity. In 2021, three thiophene-based COFs (COF-NUST-7, 8, 9) were first demonstrated, which were further served as hosts to accommodate ILs and lithium salt for fast Li^+ conduction (Figure 6).[92] All the COFs showed good crystallinity, and the PXRD patterns at variable temperatures revealed the crystallinity of COFs well maintained until 180 ºC. The BET surface areas for COF-NUST-7, 8, 9 are 1214, 92 and 95 m^2 g^{-1}, respectively. The COF based solid composite electrolytes (SCEs) were prepared by pressing into pellets. And the SCE powders were obtained by doping COFs with IL (1-butyl-1-methylpyrrolidinium bis(trifluoromethanesulfonyl)imide) and lithium salt (LiTFSI) at different weight ratios to obtain IL-x@NUST-COF (x = 0.25, 0.5, 0.75, and 1.0, respectively). With increasing the x values, the corresponding conductivities showed obvious increase, and the E_a exhibited negligible changes. IL-1.0@NUST-7 has the highest conductivities of 9.66×10^{-4} S cm^{-1} at 120 ºC, with E_a of 0.317 eV. The Li^+ conductivities of IL-1.0@NUST-9 and IL-1.0@NUST-8 are 2.60×10^{-3} and 1.40×10^{-3} S cm^{-1} at the same temperature, respectively. The higher conductivity may be attributed to the low surface areas of NUST-8 and NUST-9, making IL and LiTFSI exist in the powders gap rather than in pores. More importantly, the all-solid battery based on IL-1.0@NUST-7 showed much more stable charge and discharge behavior than the solid battery with PEO as electrolytes at 100 ºC, indicating smooth and steady ionic conducting pathways from a high structural thermal stability of COFs.

n POLYELECTROLYTE COFS FOR LITHIUM ION CONDUCTION

Poly(ethylene oxide)-based electrolytes (PEO) are now becoming increasingly attractive as solid polymer electrolytes, because of their excellent properties such as safety, mechanical properties, and flexibility. However, PEO hardly meets these requirements since it is highly crystalline at low temperature and forms a rigid structure that greatly impedes ion motion. To overcome the limitation, many researches have been done including synthesizing grafted PEO copolymer, preparing crosslinking networks or copolymers. However, the resultant polymer electrolytes lack optimizing ion diffusion pathway, hindering the lithium ion transport fast. Thus, preparing the solid electrolytes with well-defined pore structure for ion transport may have a chance

DOI: 10.14102/j.cnki.0254-5861.2022-0114

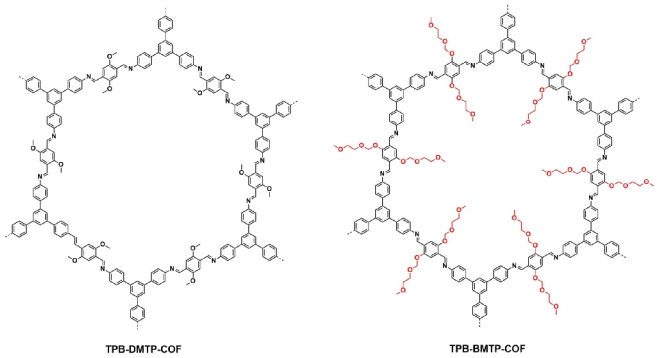

Figure 7. Chemical structures of TPB-DMTP-COF and TPB-BMTP-COF.

to solve the issues of PEO-based electrolytes. Unfortunately, it is difficult to dissociate ionic bonds and to transport lithium ions even if lithium salts are loaded within the bare pores of a porous material.

In 2018, Jiang's group first reported polyelectrolyte COFs with linking short PEO chains along the pore walls through covalent bonds.[93] The polyelectrolyte COF (TPB-BMTP-COF) with flexible oligo (ethylene oxide) chains on the channel walls was synthesized from TPB and BMTP monomers, and TPB-DMTP-COF was synthesized under the same condition, which holds methoxyl groups on the edge phenyl units (Figure 7). TPB-DMTP-COF displayed a surface area of 2458 $m^2 g^{-1}$, and a pore volume of 1.34 $cm^3 g^{-1}$. With replacing methoxyl groups with oligo (ethylene oxide) chains, the surface declined to 1746 $m^2 g^{-1}$, with a pore value of 0.96 $cm^3 g^{-1}$. The pore size reduced from 3.26 to 3.02 nm. TPB-BMTP-COF did not decompose below 300 ºC, indicating its high thermal stability. In addition, the crystallinity and porosity can be well retained even treated with $LiClO_4$ in the pores and exposed in the air over one month. Encouraged with uniform distribution of oligo (ethylene oxide) chains in 1D channels and excellent stability, the COF was loaded with $LiClO_4$ (Li^+@TPB-BMTP-COF) for lithium ion conduction. Compared to Li^+@TPB-DMTP-COF, the corresponding ion conductivities were evaluated to be 6.04 × 10^{-6}, 2.85 × 10^{-5} and 1.66 × 10^{-4} S cm^{-1}, which are 44, 42 and 30 times higher than those of Li^+@TPB-DMTP-COF. Notably, the ion conductivity at 90 °C reaches 5.49 × 10^{-4} S cm^{-1}. The conductivity was retained even after 24 hours at 90 °C. These results are remarkable because the ion conductivity of PEO-Li^+ complex is only 8.0 × 10^{-8} S cm^{-1} at 40 °C. The E_a values for TPB-BMTP-COF and TPB-DMTP-COF are 0.87 and 0.96 V, indicating lithium ion transport in the channels via vehicle mechanism. Compared to Li^+@TPB-DMTP-COF, the greatly enhanced ion conductivity observed for Li^+@TPB-BMTP-COF originates from the presence of dense oligo (ethylene oxide) chains that form a polyelectrolyte interface in the channels upon complexation with lithium ions. This built-in interface facilitates the dissociation of ionic bond and offers a pathway for lithium ion transport between the neighboring oligo (ethylene oxide) chains. These results indicate that engineering a polyelectrolyte interface in the channels is of substantial importance for designing ion-conducting COFs.

To introduce dense and flexible PEO groups into the frameworks, a direct self-assembly approach that involves preorganization of functional groups into the building blocks has been adopted. Three PEO-functionalized hydrazone-linked COFs were synthesized from 1,3,5-triformylbenzene with three PEO based hydrazide monomers of different length. The COFs are denoted as COF-PEO-X (X = 3, 6, and 9), in which X is the number of PEO units (Figure 8a).[94] All COFs adopted an eclipsed AA stacking model. The crystallinity exhibited slight decrease due to the expansion of layer space. COF-PEO-X showed high thermal stability until 300 ºC. The chains in the pores made COFs have low BET surface areas. And corresponding BET surface areas for COF-PEO-(3, 6, 9) are 13, 4, and 5 $m^2 g^{-1}$, whereas the analogous COF-42 without PEO chains has a BET surface area of 748 $m^2 g^{-1}$. Thus, the inner pores of COFs were fully occupied with PEO chains, which is beneficial for lithium ion conduction. DSC measurements showed the melting temperature for COF-PEO-3 is 89 °C, and COF-PEO-6 and COF-PEO-9 displayed glass transitions (Tg) of -57 and -62 °C, which suggested that the PEO chains in COF-PEO-6 and COF-PEO-9 are in quasi-liquid state. The variable temperature PXRD pattern revealed that the crystalline structure of framework in COF-PEO-6 employed negligible

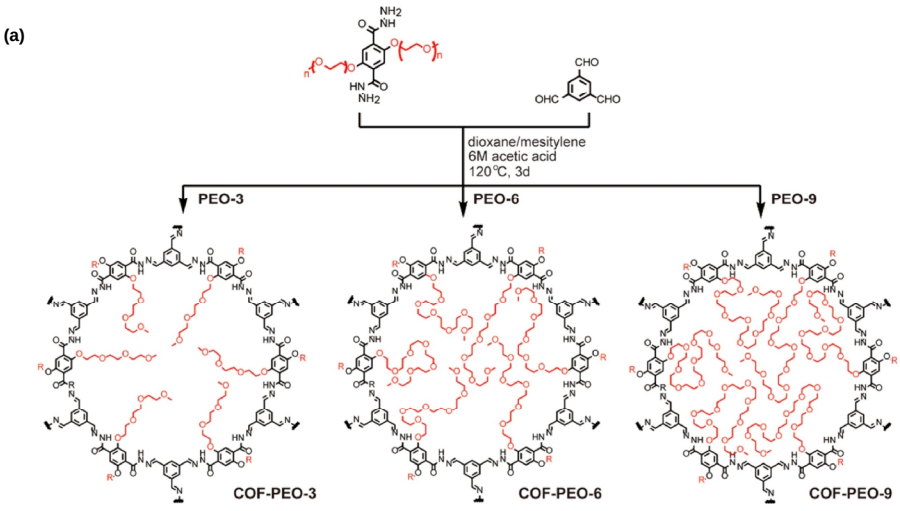

Chin. J. Struct. Chem. **2022**, 41, 2211003-2211017
DOI: 10.14102/j.cnki.0254-5861.2022-0114

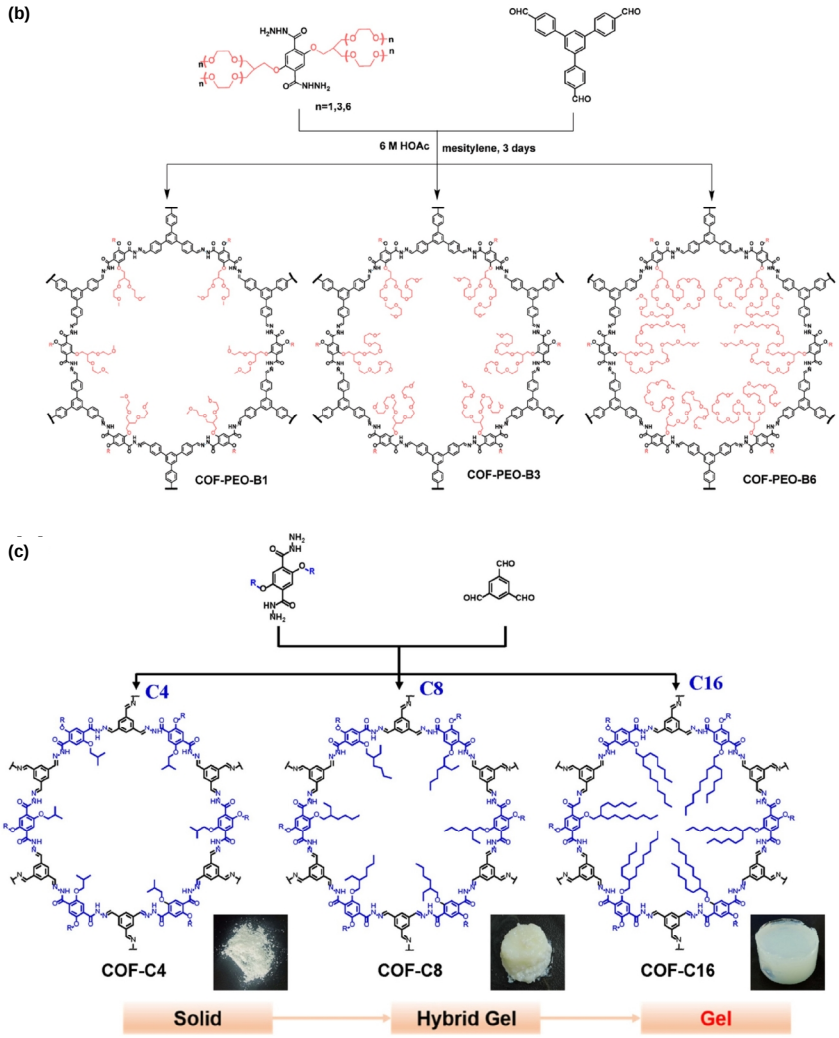

Figure 8. (a) Synthesis of COF-PEO-x (x = 3, 6, 9). Reproduced with permission from ref. 94. (b) Synthesis of COF-PEO-BX (x = 1, 3, 6). Reproduced with permission from ref. 95. (c) Synthesis of COF-CX (x = 4, 8, 16). Reproduced with permission from ref. 96.

thermal expansion. The temperature dependence solid state ^{1}H NMR spectra are indicative of mobile PEO chains anchored on the rigid framework. The COF-PEO-X was treated with LiTFSI solution (THF), and the weight ratios of O and Li are 8.8/1, 7.5/1 and 5.9/1 in COF-PEO-3, 6, and 9, respectively. The T_g for COF-PEO-6 and 9 increased to 27 and 32 ºC because of the complexation of Li^+ with polar PEO units by intra- or interchain interactions, thereby decreasing the mobility of PEO. The longer chains in COFs result in higher conductivity. The conductivities at 200 °C for COF-PEO-3-Li, COF-PEO-6-Li and COF-PEO-9-Li are 9.72 × 10^{-5}, 3.71 × 10^{-4} and 1.33 × 10^{-3} S cm^{-1}, respectively, whereas that for COF-42-Li lacking PEO chains in the pore is 1.77 × 10^{-8} S cm^{-1}, about 5 orders of magnitude lower than that of COF-PEO-9-Li. The lithium ion conductive measurement for COF-PEO-X-Li was carried out from 30 to 200 °C. Nonlinear profiles of conductivity as a function of temperature are normally found for quasi-liquid PEO and other polymer electrolytes. Importantly, the conductivity of COF-PEO-9-Li was well maintained over 12 hours at 200 °C. Generally, lithium ion batteries could not work above 80 ºC because of unstable liquid electrolytes. The fabricated lithium ion batteries (Li/COF-PEO-9-Li) showed a stable working voltage of 5.2 V verse Li/Li^+ at 100 ºC. The capacity achieved 120 mAh g^{-1} and became stable over 10 cycles. The all solid batteries proved that COF-PEO-X-Li acted as solid electrolytes with thermal and electrochemical stability.

To avoid anion conduction and increase the Li-ion transference number, the branched PEG chains were anchored into the pore surface of COFs.[95] Three PEG-functionalized COFs (COF-PEG-B1, COF-PEG-B3, and COF-PEG-B6) were synthesized from 1,3,5-tris(4-formyl-phenyl)-benzene with three PEG-based hydrazide monomers of different lengths (Figure 8b). The as-obtained COFs showed stable crystallinity from 40 to 200 ºC. The DSC curves showed COF-PEG-B1 does not give rise to any endothermic peaks, whereas the T_g for COF-PEG-B3 and COF-PEG-B6 are -1 and -38 °C, illustrating the increasing chain length which results in more intense segment movement. The LiTFSI was then loaded in the pores of COFs to obtain COF-PEG-B1, B3 and B6-Li, respectively. The conductivities of

DOI: 10.14102/j.cnki.0254-5861.2022-0114

COF-PEG-B1-Li are 2.3 × 10^{-8}, 4.7 × 10^{-6} and 3.3 × 10^{-5} S cm^{-1} at 60, 140, and 200 °C, respectively. The conductive performance was improved, with the increasing length of PEG chains. The COF-PEG-B3-Li and COF-PEG-B6-Li have conductivities of 1.6 × 10^{-4} and 1.5 × 10^{-3} S cm^{-1} at 200 °C, respectively. The conductivity of COF-PEG-B6-Li was kept about 10^{-3} S cm^{-1} at 200 °C for 48 h. The corresponding E_a for COF-PEG-B6-Li is 0.60 eV, which is lower than the values of COF-PEG-B1-Li (0.74 eV) and COF-PEG-B3-Li (0.71 eV). In addition, COF-PEG-B6-Li has higher T_{Li^+} of 0.30 than COF-PEG-B1-Li and COF-PEG-B3-Li because the most crowded PEG chain in it can inhibit $TFSI^-$ movement in a certain direction. With using COF-PEG-B6-Li as the electrolyte, the solid battery exhibited a capacity retention of 87% after 60 cycles, confirming its satisfied stability.

Although the polyelectrote COFs have been well developed by using functional building units or pore surface engineering, the insoluble and infusible crystalline powders with poor processability hindered their further practical applications. Polymer gel electrolytes (PGEs) have been developed for various electrochemical devices because they have no solvent leakage and evaporation features. Recently, a general side-chain engineering strategy to construct gel-state COFs with high processability has been demonstrated.[96] The COFs (COF-Cx) with different lengths of branched alkyl chains were synthesized, where the branched x (x = 4, 8, or 16) are the number of carbon atoms comprised by the hydrazide-based monomers (Figure 8c). With increasing the length of alkyl chains, the state of COFs became the gel morphology from the solid. The COF-C4 is stacked in an AA stacking model with good crystallinity. With increasing the length, the peak position for 110 facet exhibited positive shift, indicating smaller pore size. The NMR spectra showed the interlayer interaction for COF-C16 is smaller than that of COF-C4, and the mobility of chains enhanced when the frameworks are in gel state. Concerning the excellent high machinability and flexibility, the COF-gel can be cut in specific shapes and thickness. The full cell based on the COF-gel showed higher capacity at the same current density and better long-term stability than that without COF-gel.

Apart from using functional skeletons, pore surface engineering is another effective method to synthesize functional COFs. It allows the controlled functionalization of COF pore walls with organic groups, by which the contents and functions can be tuned.[97] The capability of designing pore channels renders COFs able to design outstanding properties ranging from heterogeneous catalysis to gas absorption and energy storage. By this method, a series of COFs with different PEO chains (length and density) have been designed and synthesized for lithium ion conduction. TPB-DMTP-COF and TPB-TP-COF worked as the base skeleton for constituting various polyelectrolyte interfaces 1D channels (Figure 9). And TPB-BMTP-COF (Figure 7) with bis(2-methoxyethyl)ether polyelectrolyte units (TriEO, $C_6H_{12}O_3$) on walls has also been developed. The pore surface engineering to integrate different density of tetra (ethylene oxide) polyelectrolyte units (TEO; $C_8H_{17}O_4$) to the pore walls of TPB-DMTP-COF and TPB-BMTP-COF was used to develop two series of COFs whose walls are engineered with methoxy/TEO or TriEO/TEO

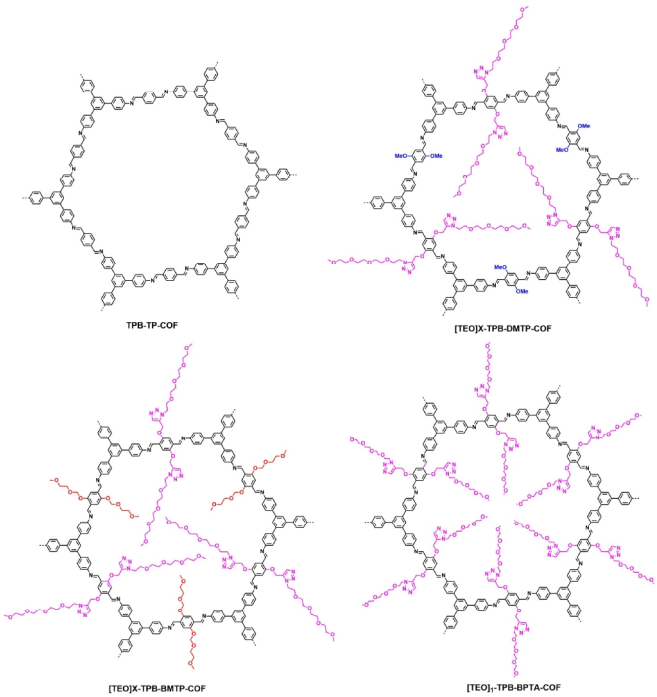

Figure 9. Schematic of TPB-TP-COF, $[TEO]_X$-TPB-DMTP-COFs. $[TEO]_X$-TPB-BMTP-COFs and $[TEO]_1$-TPB-BPTA-COF. The X values are 0.33 and 0.5.

sequences at designated ratios. By tuning the molar ratio of BPTA to DMTP or BMTP, the resulting COFs, i.e. $[HC{\equiv}C]_X$-TPB-DMTP-COFs and $[HC{\equiv}C]_X$-TPB-BMTP-COFs, possess discrete contents of ethynyl units on the pore walls. The X value is determined by X = [BPTA]/([BPTA]+[DMTP]) or [BPTA]/([BPTA]+[BMTP]) and is designated to be 0.33 and 0.5. After condensation, $[HC{\equiv}C]_X$-TPB-DMTP-COFs, $[HC{\equiv}C]_X$-TPB-BMTP-COFs and TPB-BPTA-COF were reacted via click reaction of the ethynyl units with 13-azido-2,5,8,11-tetraoxatridecane to anchor the TEO units to the pore walls to yield five new COFs, including $[TEO]_{0.33}$-TPB-DMTP-COF, $[TEO]_{0.5}$-TPB-DMTP-COF, $[TEO]_{0.33}$-TPB-BMTP-COF, $[TEO]_{0.5}$-TPB-BMTP-COF and $[TEO]_1$-TPB-BPTA-COF. All the COFs have good crystallinity, and adopt AA stacking model. Both of $[TEO]_X$-TPB-DMTP-COFs and $[TEO]_X$-TPB-BMTP-COFs were thermally stable before 260 ºC under N_2. With increasing the TEO density in the frameworks, the BET surface areas are decreased. For example, $[TEO]_{0.33}$-TPB-BMTP-COF and $[TEO]_{0.5}$-TPB-BMTP-COF exhibited decreased porosities by showing BET surface areas of 633 and 78 m^2 g^{-1}, pore volumes of 0.39 and 0.09 cm^3 g^{-1} and pore sizes of 2.73 and 2.67 nm, respectively. $LiClO_4$ was then loaded into the pores to obtain Li^+@COFs. The conductive performance was invesitgated from 40 to 90 °C. Among these Li^+@COFs, the Li^+@$[TEO]_{0.5}$-TPB-DMTP-COF exhibited the highest ion conductivities of 1.31 × 10^{-5}, 7.32 × 10^{-5} and 2.49 × 10^{-4} S cm^{-1} at 40, 60 and 80 °C. The conductivity for Li^+@$[TEO]_{0.5}$-TPB-DMTP-COF can be maintained over 48 hours at 90 °C. Moreover, the E_a value of Li^+@$[TEO]_{0.5}$-TPB-DMTP-COF is 0.68 eV, smaller than those of Li^+@TPB-DMTP-COF

Chin. J. Struct. Chem. **2022**, 41, 2211003-2211017
DOI: 10.14102/j.cnki.0254-5861.2022-0114

(0.96 eV) and Li^+@$[TEO]_{0.33}$-TPB-DMTP-COF (0.78 eV). In order to get insight into the role of polyelectrolyte chain and exclude the effect of ion concentration, the ion conductivity with the ion content was normalized. By integrating the TEO units onto the pore walls, the ion mobility is sharply enhanced by 336 and 1490 times for Li^+@$[TEO]_{0.33}$-TPB-DMTP-COF and Li^+@$[TEO]_{0.5}$-TPB-DMTP-COF, respectively, indicating that the TEO units are much more efficient than the methoxyl groups (2.1) in promoting ion transport. This strategy enables a quantitative correlation between interface and ion transport.

n IONIC COFS FOR LITHIUM ION CONDUCTION

In addition to introducing polyelectrolyte groups along the pore walls, constructing ionic COFs is another effective method to boost lithium ion conduction in the pore channels.

In 2015, Zhang *et al.* have synthesized ionic COFs (ICOF-1 and ICOF-2) with different $[Me_2NH_2]^+$ and Li^+ in the skeletons via spiro-borate linkage, respectively (Figure 10a).[98] Both of ionic COFs have high surface areas of 1022 for ICOF-1 and 1259 m^2 g^{-1} for ICOF-2 with pore sizes about 1.1 and 2.2 nm, respectively. The ICOF-2 was mixed with PVDF in a weight ratio of 2/1 to prepare a membrane, which was then soaked in propylene carbonate (PC) for 24 hours. The PC content in the membrane is about 55 wt%. The ion conductivity for the membrane achieved 3.05×10^{-5} S cm^{-1} at room temperature. Different from traditional polymer electrolytes, the conductivity is in line relationship with temperature, and the E_a for ICOF-2 is 0.24 eV. More importantly, the lithium ion transport number for ICOF-2 is about 0.8, higher than that of the traditional polymer electrolytes (about 0.5).

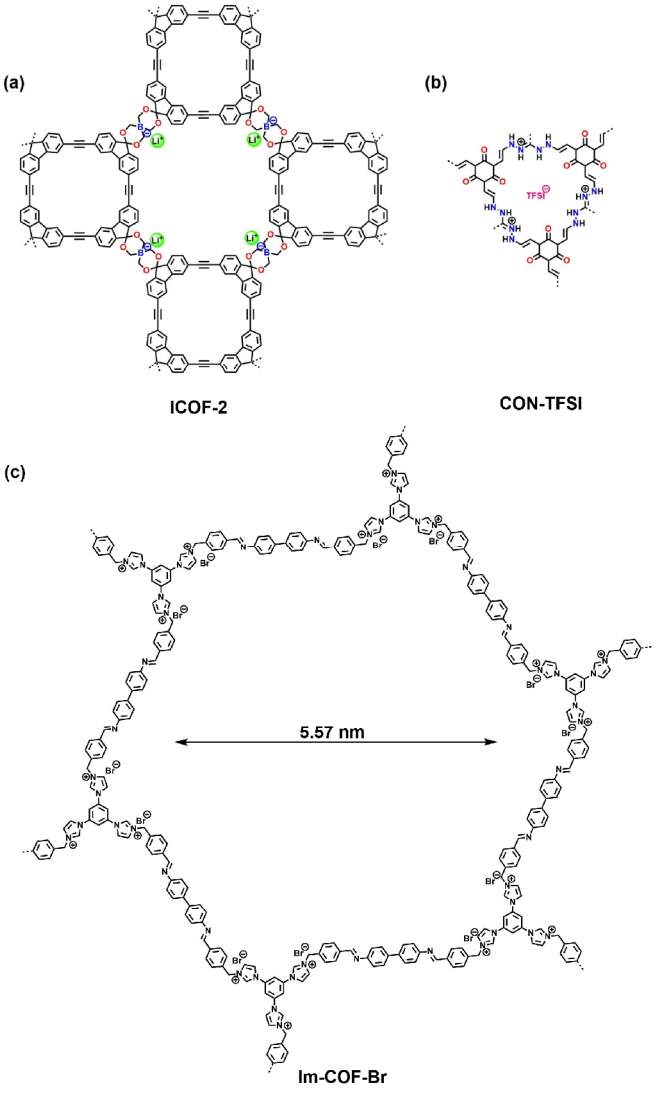

Figure 10. Chemical structures of (a) ICOF-2, (b) CON-TFSI, and (c) Im-COF-Br.

To indeed isolate the ion pairs, a cationic moiety incorporated into the skeleton of a COF material has been synthesized. The 2D COF nanosheet with chloride counterions (CON-Cl) was first synthesized, with the Cl anion replaced by TFSI anion (bis(trifluoromethane) sulfonamide) by ion exchange methods to form CON-TFSI. Finally, CON-TFSI has been mixed with LiTFSI to obtain Li-CON-TFSI (Figure 10b).[99] Li-CON-TFSI displayed loose layers with thickness of 5 nm. The Li-CON-TFSI exhibited a conductivity of 5.74×10^{-5} S cm^{-1} at 30 ºC and 2.09×10^{-4} S cm^{-1} at 70 ºC, with an E_a of 0.34 eV. The working voltage was revealed by linear sweep voltammetry (LSV) measurement. No obvious decomposition of any components occurs until 3.8 V versus Li^+/Li. The solid ^{7}Li NMR suggested that the lithium is in different chemical environments for Li-CON-TFSI compared with pure LiTFSI. The cationic framework can interact with TFSI anion by electrostatic forces, thereby liberating lithium ion for fast transport. Moreover, Fourier transform infrared spectra (FT-IR) disclosed that the carbonyl coordination provides abundant sites for Li^+ transport and thus also contributes to the Li^+ conductivity.

Similarly, 2D imidazolium-based ionic-COF has been synthesized by solvothermal method.[100] Im-COF-Br has a BET surface area of 90 m^2 g^{-1} and a pore volume of 0.14 cm^3 g^{-1} (Figure 10c). The pore size of Im-COF-Br was 5.57 nm. Br anion in Im-COF-Br was then substituted with TFSI anion to yield Im-COF-TFSI through ion exchange method. Im-COF-TFSI was thermally stable below 300 ºC under N_2. Im-COF-TFSI was then loaded with LiTFSI (Im-COF-TFSI@Li) as the solid electrolyte. The conductive measurement was carried out from 303 to 353 K. The conductivity was 2.92×10^{-5} S cm^{-1} at 303 K, which increased to 4.04×10^{-4} S cm^{-1} at 353 K. The conductivities for Im-COF-Br@Li are 8.34×10^{-7} and 3.63×10^{-5} S cm^{-1} at 303 and 353 K, respectively. The superior conductive performance for Im-COF-TFSI@Li was caused by the highly hydrophobic properties of $TFSI^-$ that would benefit for higher ion conductivity obviously. The E_a values calculated from Arrhenius plot for COF-TFSI@Li and Im-COF-Br @Li are 0.32 and 0.61 eV. Thus, Im-COF-TFSI@Li migrated along the channels in hopping mechanism, whereas the mechanism for Im-COF-Br@Li was in vehicle mechanism. The electrochemical window for Im-COF-TFSI@Li is about 4.2 V, indicating its good electrochemical stability. The lithium ion battery fabricated with Im-COF-TFSI@Li as electrolyte displayed a stable voltage curve over 300 hours at 0.02 and 0.10 mA cm^{-2}, demonstrating Im-COF-TFSI@Li has a stable interface of Li metal.

DOI: 10.14102/j.cnki.0254-5861.2022-0114

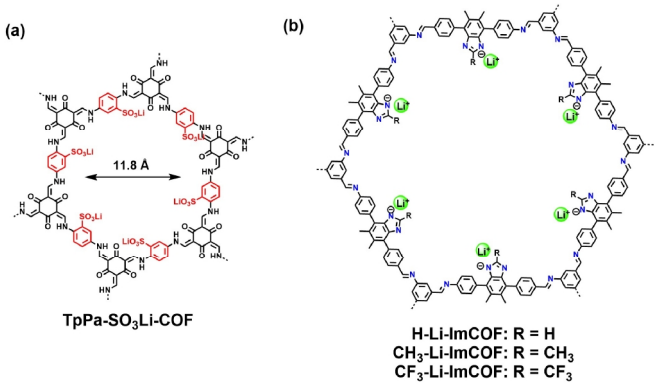

Figure 11. Chemical structures of (a) TpPa-SO_3Li-COF and (b) H-Li-ImCOF, CH_3-Li-ImCOF, and CF_3-Li-ImCOF.

In lithium ion batteries, both anion and cation are mobile in the liquid or solid eletrolytes. In charge/discharge process, the anions tend to accumulate at the anode side and cause concentration gradients, which resulted in poor performance of batteries, including voltage loss, high internal impedance and undesirable reactions.[101-104] Therefore, developing single-ion conductors is highly desirable to overcome the challenges and drawbacks of dual-ion conducts. Concerning the designable feature of COFs, a single lithium-ion conductive COF (TpPa-SO_3Li) has been synthesized (Figure 11a).[105] The COF constructed anionic frameworks, and the SO_3^- groups were distributed along the hexagonal pores. The TpPa-SO_3H-COF was first synthesized, which was then reacted with LiOAc to exchange the proton with lithium ions. The lithium content of 2.31 wt% is close to the calculated one (2.33 wt%). The BET surface area of TpPa-SO_3Li is 348 m^2 g^{-1}, with a pore size of 1.18 nm. The smaller pore size compared with other COFs may contribute high lithium ion density in the pores. The MAS ^{7}Li NMR spectrum confirmed the lithium ion is in an identical environment, and the spin-lattice relaxation time is about 1.91 s, demonstrating that lithium ion migrates fast in the pores. The conductive performance was evaluated from room temperature to 110 ºC. TpPa-SO_3Li achieved a high conductivity of 2.7 × 10^{-5} S cm^{-1} at room temperatue. The Arrhenius plot shows the E_a of 0.18 eV, implying hopping mechanism (Figure 11a). TpPa-SO_3Li showed a high T_{Li}^+ value of 0.9, indicating that predominant contribution of conductivity was from lithium ion. The DFT calculation revealed that the lithium ion transport in the axial pathway required much lower migration barriers than that in planar one due to the shorter hopping distance. The Li-ion intermediates combining oxygen of SO_3^- groups in channels displayed higher thermodynamic stability than that in planar pathway. Moreover, TpPa-SO_3Li displayed excellent thermal stability over 200 °C, and electrochemical stability with voltage window of 4 V. The all solid state battery with TpPa-SO_3Li as electrolyte has been fabricated, which is stable over 320 h without an appreciable increase and an irreversible fluctuation of over-potential. Notably, the random Li deposition was hardly observed after cycling, further confirming the TpPa-SO_3Li enhanced the stability of the battery.

Pore environment has also influenced the conductive performance of single lithium-ion conductive COFs. Recently, a series of single-ion conducting imidazolate ICOFs have also been reported for lithium ion conduction. With linking different substituents (H, CH_3, CF_3) on the imidazolate backbones, the conductive properties can be tuned. H-ImCOF, CH_3-ImCOF and CF_3-ImCOF with different substituents (R = H, CH_3, and CF_3) on the imidazole ring were first synthesized, which were then treated with n-BuLi to introduce lithium on the imidazole frameworks (H-Li-ImCOF, CH_3-Li-ImCOF, and CF_3-Li-ImCOF) (Figure 11b).[106] The lithium contents in H-Li-ImCOF, CH_3-Li-ImCOF, and CF_3-Li-ImCOF are 3.2%, 1.7%, and 1.4%, respectively. All of COFs displayed good crystallinity and adopted AA stacking model. The BET surface area of H-Li-ImCOF is 350 m^2 g^{-1}, with a total pore volume of 0.59 cm^3 g^{-1}. H-Li-ImCOF, CH_3-Li-ImCOF, and CF_3-Li-ImCOF displayed slight weight loss of 8%, 15% and 15% before 450 °C. Li-ImCOFs were then pressed into pellets, and soaked into propylene carbonate (PC) for conductivity measurement. The lithium contents for H-Li-ImCOF, CH_3-Li-ImCOF, and CF_3-Li-ImCOF are 2.7%, 1.4%, and 1.1% with PC uptake. The conductivities for H-Li-ImCOF, CH_3-Li-ImCOF, and CF_3-Li-ImCOF are 5.3 × 10^{-3}, 8.0 × 10^{-5} and 7.2 × 10^{-3} S cm^{-1}. The linear Arrhenius plot was obtained from room temperature to 85 ºC, from which the E_a values are 0.12, 0.27, and 0.10 eV for H-Li-ImCOF, CH_3-Li-ImCOF, and CF_3-Li-ImCOF. The corresponding T_{Li}^+ values are 0.88, 0.81 and 0.93. And the electrochemical stability windows for Li-ImCOFs is about 4.5 V. The lithium ion batteries based on Li-ImCOFs achieved cycle stability at room temperature, confirming the potential of Li-ImCOFs as solid electrolyte materials. As a comparison, unlithiated parent H-ImCOF was mixed with $LiClO_4$ and PC (H-Li-ImCOF) for conductive test. The conductivity for H-Li-ImCOF is about 4 × 10^{-5} S cm^{-1}, with a low T_{Li}^+ of 0.21, which is almost 2 orders of magnitude lower than that of H-Li-ImCOF. This result confirmed the roles of anion immobilization on the framework. The different conductive behavior for H-Li-ImCOF, CH_3-Li-ImCOF, and CF_3-Li-ImCOF was dependent on the electronic properties of the substituents. For example, the electron-withdrawing groups helped form loose ion pairs with lithium cations, leading to higher lithium ion conductivity. These substituent effects were studied by ^{7}Li solid-state NMR spectra. The positions of ^{7}Li resonance signals for CH_3-Li-ImCOF, H-Li-ImCOF, and CF_3-Li-ImCOF were at 1.65, 1.33 and -0.25 ppm, and the high-field shift of the last one was due to the

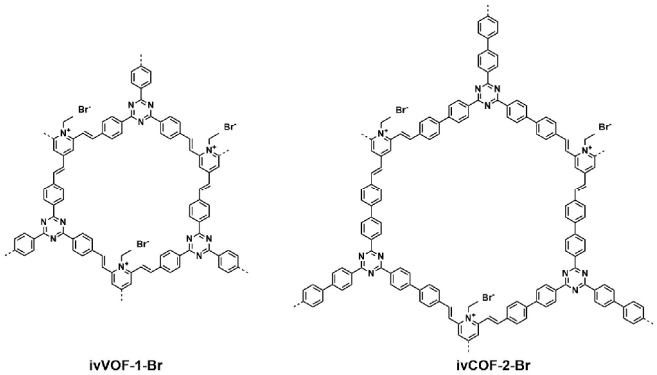

Figure 12. Chemical structures of iv-COF-1-Br and iv-COF-2-Br linked by C=C bonds.

DOI: 10.14102/j.cnki.0254-5861.2022-0114

Table 1. Summary of Typical Performance for COFs-Based Lithium Ion Electrolytes at Room Temperature

COFs	Lithium salts	Solvents	Lithium ion conductivity [S/cm] at RT	Ea [eV]	Lithium ion transport number [t_{Li^+}]	Ref.
Tppa-1 COF	$LiClO_4$	THF	1.50×10^{-4}	/	/	87
COF-5	$LiClO_4$	THF	2.60×10^{-4}	0.037	/	87
DBC-2P⊂PEG-$LiBF_4$	$LiBF_4$	/	6.16×10^{-9}	0.09	/	88
PEG-Li^+@CD-COF-Li	$LiClO_4$	/	2.60×10^{-5}	0.17	0.2	89
PEG-Li^+@COF-300	$LiClO_4$	/	1.40×10^{-6}	0.20	0.44	89
PEG-Li^+@COF-5	$LiClO_4$	/	3.60×10^{-8}	0.35	0.40	89
PEG-Li^+@EBCOF-ClO_4	$LiClO_4$	/	1.93×10^{-5}	0.21	0.60	89
PEG-Li^+@Spe	LiTFSI	/	3.40×10^{-8}	0.51	/	90
PEG-Li^+@COF-M	LiTFSI	/	2.20×10^{-5}	0.46	/	90
3D-SpCOF-SSE	LiTFSI	/	6.40×10^{-4}	0.13	0.70	91
3D-SpCOF-OH-SSE	LiTFSI	/	1.21×10^{-3}	0.03	0.64	91
IL-1.0@NUST-7	LiTFSI	/	9.66×10^{-4} (120 °C)	0.317	/	92
IL-1.0@NUST-8	LiTFSI	/	1.40×10^{-3} (120 °C)	0.301	/	92
IL-1.0@NUST-9	LiTFSI	/	2.60×10^{-3} (120 °C)	0.323	/	92
Li^+@TPB-BMTP-COF	$LiClO_4$	/	6.04×10^{-6}	0.87	/	93
COF-PEO-3-Li	LiTFSI	THF	9.72×10^{-5} (200 °C)	/	/	94
COF-PEO-6-Li	LiTFSI	THF	3.71×10^{-4} (200 °C)	/	/	94
COF-PEO-9-Li	LiTFSI	THF	1.33×10^{-3} (200 °C)	/	/	94
COF-PEG-B1-Li	LiTFSI	/	3.3×10^{-5} (200 °C)	0.74	/	95
COF-PEG-B3-Li	LiTFSI	/	1.6×10^{-4} (200 °C)	0.71	0.18	95
COF-PEG-B6-Li	LiTFSI	/	1.5×10^{-3} (200 °C)	0.60	0.30	95
Li+@$[TEO]_{0.5}$-TPB-DMTP-COF	$LiClO_4$	/	1.31×10^{-5}	0.68	/	97
ICOF-2	/	PC	3.05×10^{-5}	0.24	0.8	98
Li-CON-TFSI	LiTFSI	/	5.74×10^{-5}	0.34	0.61	98
Im-COF-Br@Li	LiTFSI	/	8.34×10^{-7}	0.61	/	99
Im-COF-TFSI@Li	LiTFSI	/	2.92×10^{-5}	0.32	0.62	99
TpPa-SO_3Li	LiOAc	/	2.7×10^{-5}	0.18	0.9	105
H-Li-ImCOF	n-BuLi	PC	5.3×10^{-3}	0.12	0.88	106
CH_3-Li-ImCOF	n-BuLi	PC	8.0×10^{-5}	0.27	0.81	106
CF_3-Li-ImCOF	n-BuLi	PC	7.2×10^{-3}	0.10	0.93	106
Li/PEO@ivCOF-1-Br	LiTFSI	/	4.17×10^{-4}	0.094	/	107
Li/PEO@ivCOF-2-Br	LiTFSI	/	3.84×10^{-4}	0.11	/	107

lengthening of the Li-N distance and diminishing solid-state ion pairing, thereby resulting in higher lithium ion mobility.

Apart from boron- and nitrogen-based linkages in COFs, the former is getting more attention due to their more stable characters. In 2021, a new family of ionic vinylene-linked two-dimensional (2D) COFs through the Knoevenagel condensation were reported.[107] The iv-COF-1-Br and iv-COF-2-Br were synthesized from *N*-ethyl-2,4,6-trimethylpyridinium bromide (ETMP-Br) with tritopic aromatic aldehyde derivatives 1,3,5-tris(4-formylphenyl) triazine (TFPT) and 1,3,5-tris-(4′-formyl-biphenyl-4-yl)triazine (TFBT), respectively (Figure 12). The PXRD patterns showed both COFs have good crystallinity and are stacked in AA model, and their crystal structures are retained even in NaOH (14 M) and HCl (12 M) aqueous solutions, respectively. The iv-COF-1-Br and iv-COF-2-Br have BET surfaces of 873 and 1343 $m^2\ g^{-1}$, with corressponding pore sizes of 1.4 and 1.9 nm, respectively. Complexing prepared COFs with LiTFSI and PEO through solution impregnation formed the flexible films Li/PEO@ivCOF-1-Br and Li/PEO@ivCOF-2-Br for lithium ion conduction, with their ion conductivities to be 4.17×10^{-4} and 3.84×10^{-4} S cm^{-1} at 20 ºC, respectively. And the corresponding E_a values are 0.094 and 0.11 eV, respectively. The solid-state ^{7}Li NMR spectra confirmed the lithium ion transport along the 1D channels of COFs.

To investigate the performance of batteries with COF as the electrolytes, the ionic COF (LiCOF) used a host to load liquid electrolyte to yield DMA@LiTFSI-mediated COF (DLC).[108] The liquid electrolyte was designated as DMA@LiTFSI composed of 2 M LiTFSI in dimethylacrylamide (DMA). The functional groups of flexible DMA chains could release Li^+ ions from the rigid COF backbone and simultaneously decouple the lithium salt. The Li-COF has a BET surface area of 508 $m^2\ g^{-1}$, which showed obvious decline with increasing the contents of DMA@LiTFSI. And the DSC spectra revealed the Tg for DMA@LiTFSI was higher than that of bulk DMA@LiTFSI, confirming the interaction between the host and guest. The molecular dynamics (MD) simulations showed the anionic mobility in the channels was restricted, while the anion conduction in DMA@LiTFSI was freedom. The DLC has a conductivity of 1.65×10^{-4} S cm^{-1}, about 20 times higher than that of LiCOF. The corresponding T_{Li+} is 0.85, whereas that of pure DMA@LiTFSI is 0.32. Based on the DLC

DOI: 10.14102/j.cnki.0254-5861.2022-0114

electrolyte, a Li|Li symmetric cell is stable for 450 h at a current density of 0.3 mA cm^{-2}. Moreover, a full cell with $LiFePO_4$ as a model cathode was fabricated with DLC as electrolyte. The battery showed high capacity, good rate performance and excellent stability (the capacity of 96 mA g^{-1} after 140 cycles).

n CONCLUSION

Recently, lithium ion conductivity in COFs has attracted great concerns because of their potential applications in lithium ion batteries. Compared with other polymers, COFs have many advantages in ion conductive fields. Firstly, the frameworks of COFs displayed excellent thermal and chemical stability, which is the foundation for ion conductive materials in harsh condition. The 1D channels in COFs compared with disordered pores in other porous polymers provide fast pathway for proton and lithium ion transport. In addition, the different linkages can offer binding sites with anions of proton or lithium ion sources. Moreover, the frameworks constructed with various binding blocks can be tuned and serve as proton or lithium ion carriers. Importantly, the pore environment can be functionalized by bottom-up or post-synthesis method to promote ion conduction.

In the past years, there are lots of achievements for lithium ion conduction in COFs (Table 1). The lithium ion conductive performance in COFs not only depends on the porous environments but also framework-structures. By tuning the pores or skeletons, the conductivity, conductive mechanism, and lithium ion transport were well controlled. However, COFs as conductive materials are still far from industrial applications. There are still challenges to overcome in this area. The high-cost for building units is one of the major blocks. And most COFs with high crystallinity and porosity were synthesized by solvothermal method, and how to synthesize high-quality COFs in large-scale under mild conditions is another challenge. Moreover, fabricating COFs-based membranes rather than pellets is also significant for their future application in fuel cells and solid batteries. Additionally, the conductivity for COFs at low temperature is still inferior to that of inorganic solid electrolytes (10^{-2} S cm^{-1}). There is still a long way to utilize conductive COFs in large-scale energy storage and conversion systems.

n ACKNOWLEDGEMENTS

Q. Xu acknowledges the financial support from the Natural Science Foundation of Shanghai (20ZR1464000). G. Zeng acknowledges the supports from the National Natural Science Foundation of China (21878322, 22075309) and the Science and Technology Commission of Shanghai Municipality (19ZR1479200, 22ZR1470100).

n AUTHOR INFORMATION

Corresponding authors. Emails: xuqing@sari.ac.cn (Qing Xu) and zenggf@sari.ac.cn (Gaofeng Zeng)

n COMPETING INTERESTS

The authors declare no competing interests.

n ADDITIONAL INFORMATION

Full paper can be accessed via
http://manu30.magtech.com.cn/jghx/EN/10.14102/j.cnki.0254-5861.2022-0114
For submission: https://www.editorialmanager.com/cjschem

n REFERENCES

(1) Cao, Y.; Wang, M.; Wang, H.; Han, C.; Pan, F.; Sun, J. Covalent organic framework for rechargeable batteries: mechanisms and properties of ionic conduction. *Adv. Energy Mater.* **2022**, 2200057.

(2) Zhao, X.; Pachfule, P.; Thomas, A. Covalent organic frameworks (COFs) for electrochemical applications. *Chem. Soc. Rev.* **2021**, 50, 6871-6913.

(3) Jiang, X.; Chen, Y.; Lu, C. Bio-inspired materials for photocatalytic hydrogen production. *Chin. J. Struct. Chem.* **2021**, 39, 2123-2130.

(4) Park, S.; Liao, Z.; Ibarlucea, B.; Qi, H.; Lin, H. H.; Becker, D.; Melidonie, J.; Zhang, T.; Sahabudeen, H.; Baraban, L.; Baek, C. K.; Zheng, Z.; Zschech, E.; Fery, A.; Heine, T.; Kaiser, U.; Cuniberti, G.; Dong, R.; Feng, X. Two-dimensional boronate ester covalent organic framework thin films with large single crystalline domains for a neuromorphic memory device. *Angew. Chem. Int. Ed.* **2020**, 59, 8218-8224.

(5) Evans, A. M.; Bradshaw, N. P.; Litchfield, B.; Strauss, M. J.; Seckman, B.; Ryder, M. R.; Castano, I.; Gilmore, C.; Gianneschi, N. C.; Mulzer, C. R.; Hersam, M. C.; Dichtel, W. R. High-sensitivity acoustic molecular sensors based on large-area, spray-coated 2D covalent organic frameworks. *Adv. Mater.* **2020**, 32, e2004205.

(6) Yusran, Y.; Fang, Q.; Valtchev, V. Electroactive covalent organic frameworks: design, synthesis, and applications. *Adv. Mater.* **2020**, 32, e2002038.

(7) Jin, S.; Allam, O.; Jang, S. S.; Lee, S. W. Covalent organic frameworks: design and applications in electrochemical energy storage devices. *InfoMat.* **2022**.

(8) Alahakoon, S. B.; Diwakara, S. D.; Thompson, C. M.; Smaldone, R. A. Supramolecular design in 2D covalent organic frameworks. *Chem. Soc. Rev.* **2020**, 49, 1344-1356.

(9) Guan, X.; Chen, F.; Fang, Q.; Qiu, S. Design and applications of three dimensional covalent organic frameworks. *Chem. Soc. Rev.* **2020**, 49, 1357-1384.

(10) Geng, P.; Wang, L.; Du, M.; Bai, Y.; Li, W.; Liu, Y.; Chen, S.; Braunstein, P.; Xu, Q.; Pang, H. MIL-96-Al for Li-S batteries: shape or size? *Adv. Mater.* **2022**, 34, e2107836.

(11) Li, W.; Guo, X.; Geng, P.; Du, M.; Jing, Q.; Chen, X.; Zhang, G.; Li, H.; Xu, Q.; Braunstein, P.; Pang, H. Rational design and general synthesis of multimetallic metal-organic framework nano-octahedra for enhanced Li-S battery. *Adv. Mater.* **2021**, 33, e2105163.

(12) Geng, P.; Du, M.; Guo, X.; Pang, H.; Tian, Z.; Braunstein, P.; Xu, Q. Bimetallic metal-organic framework with high-adsorption capacity toward lithium polysulfides for lithium-sulfur batteries. *Energy Environ. Mater.* **2021**, 5, 599-607.

(13) Shan, Y.; Li, Y.; Pang, H. Applications of tin sulfide-based materials in lithium-ion batteries and sodium-ion batteries. *Adv. Funct. Mater.* **2020**, 30, 2001298.

(14) Ke, S. W.; Wang, Y.; Su, J.; Liao, K.; Lv, S.; Song, X.; Ma, T.; Yuan, S.; Jin, Z.; Zuo, J. L. Redox-active covalent organic frameworks with nickel-bis(dithiolene) units as guiding layers for high-performance lithium metal batteries. *J. Am. Chem. Soc.* **2022**, 144, 8267-8277.

(15) Emmerling, S. T.; Schuldt, R.; Bette, S.; Yao, L.; Dinnebier, R. E.;

Kastner, J.; Lotsch, B. V. Interlayer interactions as design tool for large-pore COFs. *J. Am. Chem. Soc.* **2021**, 143, 15711-15722.
(16) Zhang, F.; Hao, H.; Dong, X.; Li, X.; Lang, X. Olefin-linked covalent organic framework nanotubes based on triazine for selective oxidation of sulfides with O_2 powered by blue light. *Appl. Catal. B Environ.* **2022**, 305, 121027.
(17) Li, X.; Hou, Q.; Huang, W.; Xu, H.; Wang, X.; Yu, W.; Li, R.; Zhang, K.; Wang, L.; Chen, Z.; Xie, K.; Loh, K. P. Solution-processable covalent organic framework electrolytes for all-solid-state Li-organic batteries. *ACS Energy Lett.* **2020**, 5, 3498-506.
(18) Liu, R.; Tan, K. T.; Gong, Y.; Chen, Y.; Li, Z.; Xie, S.; He, T.; Lu, Z.; Yang, H.; Jiang, D. Covalent organic frameworks: an ideal platform for designing ordered materials and advanced applications. *Chem. Soc. Rev.* **2021**, 50, 120-242.
(19) Li, X.; Yadav, P.; Loh, K. P. Function-oriented synthesis of two-dimensional (2D) covalent organic frameworks-from 3D solids to 2D sheets. *Chem. Soc. Rev.* **2020**, 49, 4835-4866.
(20) Liang, R. R.; Jiang, S. Y.; Ru-Han, A.; Zhao, X. Two-dimensional covalent organic frameworks with hierarchical porosity. *Chem. Soc. Rev.* **2020**, 49, 3920-3951.
(21) Chen, R.; Shi, J. L.; Ma, Y.; Lin, G.; Lang, X.; Wang, C. Designed synthesis of a 2D porphyrin-based sp^2 carbon-conjugated covalent organic framework for heterogeneous photocatalysis. *Angew. Chem. Int. Ed.* **2019**, 58, 6430-6434.
(22) Meng, Y.; Luo, Y.; Shi, J. L.; Ding, H; Lang, X.; Chen, W.; Zheng, A.; Sun, J.; Wang, C. 2D and 3D porphyrinic covalent organic frameworks: the influence of dimensionality on functionality. *Angew. Chem. Int. Ed.* **2020**, 59, 3624-3629.
(23) Jin, F.; Nguyen, H. L.; Zhong, Z.; Han, X.; Zhu, C.; Pei, X.; Ma, Y.; Yaghi, O. M. Entanglement of square nets in covalent organic frameworks. *J. Am. Chem. Soc.* **2022**, 144, 1539-1544.
(24) Li, Z.; Huang, N.; Lee, K. H.; Feng, Y.; Tao, S.; Jiang, Q.; Nagao, Y.; Irle, S.; Jiang, D. Light-emitting covalent organic frameworks: fluorescence improving via pinpoint surgery and selective switch-on sensing of anions. *J. Am. Chem. Soc.* **2018**, 140, 12374-12377.
(25) Wang, X.; Han, X.; Cheng, C.; Kang, X.; Liu, Y.; Cui, Y. 2D covalent organic frameworks with cem topology. *J. Am. Chem. Soc.* **2022**, 144, 7366-7373.
(26) Wang, W.; Zhao, W.; Xu, H.; Liu, S.; Huang, W.; Zhao, Q. Fabrication of ultra-thin 2D covalent organic framework nanosheets and their application in functional electronic devices. *Coord. Chem. Rev.* **2021**, 429, 213616.
(27) Mahato, M.; Tabassian, R.; Nguyen, V. H.; Oh, S.; Nam, S.; Kim, K. J.; Oh, I. sulfur- and nitrogen-rich porous π-conjugated COFs as stable electrode materials for electro-ionic soft actuators. *Adv. Funct. Mater.* **2020**, 30, 2003863.
(28) Leith, G. A.; Martin, C. R.; Mayers, J. M.; Kittikhunnatham, P.; Larsen, R. W.; Shustova, N. B. Confinement-guided photophysics in MOFs, COFs, and cages. *Chem. Soc. Rev.* **2021**, 50, 4382-4410.
(29) Hao, Q.; Zhao, C.; Sun, B.; Lu, C.; Liu, J.; Liu, M.; Wan, L. J.; Wang, D. Confined synthesis of two-dimensional covalent organic framework thin films within superspreading water layer. *J. Am. Chem. Soc.* **2018**, 140, 12152-12158.
(30) Ascherl, L.; Evans, E. W.; Gorman, J.; Orsborne, S.; Bessinger, D.; Bein, T.; Friend, R. H.; Auras, F. Perylene-based covalent organic frameworks for acid vapor sensing. *J. Am. Chem. Soc.* **2019**, 141, 15693-15699.
(31) Ying, Y.; Tong, M.; Ning, S.; Ravi, S. K.; Peh, S. B.; Tan, S. C.; Pennycook, S. J.; Zhao, D. Ultrathin two-dimensional membranes assembled by ionic covalent organic nanosheets with reduced apertures for gas separation. *J. Am. Chem. Soc.* **2020**, 142, 4472-4480.
(32) Ying, Y.; Peh, S. B.; Yang, H.; Yang, Z.; Zhao, D. Ultrathin covalent organic framework membranes via a multi-interfacial engineering strategy for gas separation. *Adv. Mater.* **2021**, e2104946.
(33) Wang, P.; Peng, Y.; Zhu, C.; Yao, R.; Song, H.; Kun, L.; Yang, W. Single-phase covalent organic framework staggered stacking nanosheet membrane for CO_2 -selective separation. *Angew. Chem. Int. Ed.* **2021**, 60, 19047-19052.
(34) Wang, Y.; Zhao, X.; Yang, H.; Bu, X.; Wang, Y.; Jia, X.; Li, J.; Feng, P. A tale of two trimers from two different worlds: a COF-inspired synthetic strategy for pore-space partitioning of MOFs. *Angew. Chem. Int. Ed.* **2019**, 58, 6316-6320.
(35) Yuan, C.; Jia, W.; Yu, Z.; Li, Y.; Zi, M.; Yuan, L. M.; Cui, Y. Are highly stable covalent organic frameworks the key to universal chiral stationary phases for liquid and gas chromatographic separations? *J. Am. Chem. Soc.* **2022**, 144, 891-900.
(36) Fu, Y.; Wu, Y.; Chen, S.; Zhang, W.; Zhang, Y.; Yan, T.; Yang, B.; Ma, H. Zwitterionic covalent organic frameworks: attractive porous host for gas separation and anhydrous proton conduction. *ACS Nano*. **2021**, 15, 19743-19755.
(37) Shevate, R.; Shaffer, D. L. Large-area 2D covalent organic framework membranes with tunable single-digit nanopores for predictable mass transport. *ACS Nano.* **2022**, 16, 2407-2418.
(38) Ding, C.; Breunig, M.; Timm, J.; Marschall, R.; Senker, J.; Agarwal, S. Flexible, mechanically stable, porous self-standing microfiber network membranes of covalent organic frameworks: preparation method and characterization. *Adv. Funct. Mater.* **2021**, 31, 2106507.
(39) Liu, Y.; Wu, H.; Li, R.; Wang, J.; Kong, Y.; Guo, Z.; Jiang, H.; Ren, Y.; Pu, Y.; Liang, X.; Pan, F.; Cao, Y.; Song, S.; He, G.; Jiang, Z. MOF-COF "alloy" membrane for efficient propylene/propane separation. *Adv. Mater.* **2022**, e2201423.
(40) Gong, Y. N.; Zhong, W.; Li, Y.; Qiu, Y.; Zheng, L.; Jiang, J.; Jiang, H. L. Regulating photocatalysis by spin-state manipulation of cobalt in covalent organic frameworks. *J. Am. Chem. Soc.* **2020**, 142, 16723-16731.
(41) Shi, J. L.; Chen, R.; Hao, H.; Wang, C.; Lang, X. 2D sp^2 carbon-conjugated porphyrin covalent organic framework for cooperative photocatalysis with TEMPO. *Angew. Chem. Int. Ed.* **2020**, 59, 9088-9093.
(42) Li, X.; Yang, S.; Zhang, F.; Zheng, L.; Lang, X. Facile synthesis of 2D covalent organic frameworks for cooperative photocatalysis with TEMPO: the selective aerobic oxidation of benzyl amines. *Appl. Catal. B Environ.* **2022**, 303, 120846.
(43) Bhunia, S.; Deo, K. A.; Gaharwar, A. K. 2D Covalent organic frameworks for biomedical applications. *Adv. Funct. Mater.* **2020**, 30, 2002046.
(44) Li, L.; Yun, Q.; Zhu, C.; Sheng, G.; Guo, J.; Chen, B.; Zhao, M.; Zhang, Z.; Lai, Z.; Zhang, X.; Peng, Y.; Zhu, Y.; Zhang, H. Isoreticular series of two-dimensional covalent organic frameworks with the kgd topology and controllable micropores. *J. Am. Chem. Soc.* **2022**, 144, 6475-6482.
(45) Peng, H.; Huang, S.; Tranca, D.; Richard, F.; Baaziz, W.; Zhuang, X.; Samori, P.; Ciesielski, A. Quantum capacitance through molecular infiltration of 7,7,8,8-tetracyanoquinodimethane in metal-organic framework/

DOI: 10.14102/j.cnki.0254-5861.2022-0114

covalent organic framework hybrids. *ACS Nano*. **2021**, 15, 18580-18589.
(46) Nguyen, H. L.; Hanikel, N.; Lyle, S. J.; Zhu, C.; Proserpio, D. M.; Yaghi, O. M. A porous covalent organic framework with voided square grid topology for atmospheric water harvesting. *J. Am. Chem. Soc.* **2020**, 142, 2218-2221.
(47) Lu, M.; Zhang, M.; Liu, C. G.; Liu, J.; Shang, L. J.; Wang, M.; Chang, J. N.; Li, S. L.; Lan, Y. Q. Stable dioxin-linked metallophthalocyanine covalent organic frameworks (COFs) as photo-coupled electrocatalysts for CO_2 reduction. *Angew. Chem. Int. Ed. En.* **2021**, 60, 4864-4871.
(48) Chen, H.; Liu, W.; Laemont, A.; Krishnaraj, C.; Feng, X.; Rohman, F.; Meledina, M.; Zhang, Q.; Van Deun, R. Leus, K.; Van Der Voort, P. A visible-light-harvesting covalent organic framework bearing single nickel sites as a highly efficient sulfur-carbon cross-coupling dual catalyst. *Angew. Chem. Int. Ed.* **2021**, 60, 10820-10827.
(49) Han, B.; Jin, Y.; Chen, B.; Zhou, W.; Yu, B.; Wei, C.; Wang, H.; Wang, K.; Chen, Y.; Chen, B.; Jiang, J. Maximizing electroactive sites in a three-dimensional covalent organic framework for significantly improved carbon dioxide reduction electrocatalysis. *Angew. Chem. Int. Ed.* **2022**, 61, e202114244.
(50) Sasmal, H. S.; Bag, S.; Chandra, B.; Majumder, P.; Kuiry, H.; Karak, S.; Sen Gupta, S.; Banerjee, R. Heterogeneous C-H functionalization in water via porous covalent organic framework nanofilms: a case of catalytic sphere transmutation. *J. Am. Chem. Soc.* **2021**, 143, 8426-8436.
(51) Liu, L.; Yin, L.; Cheng, D.; Zhao, S.; Zang, H. Y.; Zhang, N.; Zhu, G. Surface-mediated construction of an ultrathin free-standing covalent organic framework membrane for efficient proton conduction. *Angew. Chem. Int. Ed.* **2021**, 60, 14875-14880.
(52) Yang, C.; Hou, L.; Yao, Z.; Zhao, J.; Hou, L.; Zhang, L. High proton selectivity membrane based on the keto-linked cationic covalent organic framework for acid recovery. *J. Membr. Sci.* **2021**, 640, 119800.
(53) Fan, C.; Wu, H.; Guan, J.; You, X.; Yang, C.; Wang, X.; Cao, L.; Shi, B.; Peng, Q.; Kong, Y.; Wu, Y.; Khan, N. A.; Jiang, Z. Scalable fabrication of crystalline COF membranes from amorphous polymeric membranes. *Angew. Chem. Int. Ed.* **2021**, 60, 18051-18058.
(54) Sahoo, R.; Mondal, S.; Pal, S. C.; Mukherjee, D.; Das, M. C. Covalent-organic frameworks (COFs) as proton conductors. *Adv. Energy Mater.* **2021**, 11, 2102300.
(55) Wang, Z.; Yang, Y.; Zhao, Z.; Zhang, P.; Zhang, Y.; Liu, J.; Ma, S.; Cheng, P.; Chen, Y.; Zhang, Z. Green synthesis of olefin-linked covalent organic frameworks for hydrogen fuel cell applications. *Nat. Commun.* **2021**, 12, 1982.
(56) Wang, X.; Shi, B.; Yang, H.; Guan, J.; Liang, X.; Fan, C.; You, X.; Wang, Y.; Zhang, Z.; Wu, H.; Cheng, T.; Zhang, R.; Jiang, Z. Assembling covalent organic framework membranes with superior ion exchange capacity. *Nat. Commun.* **2022**, 13, 1020.
(57) Wu, M.; Zhao, Y.; Zhao, R.; Zhu, J.; Liu, J.; Zhang, Y.; Li, C.; Ma, Y.; Zhang, H.; Chen, Y. Chemical design for both molecular and morphology optimization toward high-performance lithium-ion batteries cathode material based on covalent organic framework. *Adv. Funct. Mater.* **2021**, 32, 2107703.
(58) Zhao, G.; Li, H.; Gao, Z.; Xu, L.; Mei, Z.; Cai, S.; Liu, T.; Yang, X.; Guo, H.; Sun, X. Dual-active-center of polyimide and triazine modified atomic-layer covalent organic frameworks for high-performance li storage. *Adv. Funct. Mater.* **2021**, 31, 2101019.
(59) Fu, W.; Zhang, M.; Sheng, Z. Mesh-liked carbon nanosheets intercalated into layered TiO_2 as a zero-strain anode for lithium-ion storage. *Chin. J. Struct. Chem.* **2021**, 40, 797-805.
(60) Zhao, G.; Xu, L.; Jiang, J.; Mei, Z.; An, Q.; Lv, P.; Yang, X.; Guo, H.; Sun, X. COFs-based electrolyte accelerates the Na^+ diffusion and restrains dendrite growth in quasi-solid-state organic batteries. *Nano Energy* **2022**, 92, 106756.
(61) Kong, L.; Liu, M.; Huang, H.; Xu, Y.; Bu, X. Metal/covalent-organic framework based cathodes for metal-ion batteries. *Adv. Energy Mater.* **2021**, 12, 2100172.
(62) Gu, S.; Wu, S.; Cao, L.; Li, M.; Qin, N.; Zhu, J.; Wang, Z.; Li, Y.; Li, Z.; Chen, J.; Lu, Z. Tunable redox chemistry and stability of radical intermediates in 2D covalent organic frameworks for high performance sodium ion batteries. *J. Am. Chem. Soc.* **2019**, 141, 9623-9628.
(63) Chen, X.; Zhang, H.; Ci, C.; Sun, W.; Wang, Y. Few-layered boronic ester based covalent organic frameworks/carbon nanotube composites for high-performance k-organic batteries. *ACS Nano*. **2019**, 13, 3600-3607.
(64) Zhang, W.; Ming, J.; Zhao, W.; Dong, X.; Hedhili, M. N.; Costa, P. M. F. J.; Alshareef, H. N. Graphitic nanocarbon with engineered defects for high-performance potassium-ion battery anodes. *Adv. Funct. Mater.* **2019**, 29, 1903641.
(65) Wu, X.; Chen, Y.; Xing, Z.; Lam, C. W. K.; Pang, S.; Zhang, W.; Ju, Z. Advanced carbon-based anodes for potassium-ion batteries. *Adv. Energy Mater.* **2019**, 9, 1900343.
(66) Fan, L.; Ma, R.; Zhang, Q.; Jia, X.; Lu, B. Graphite anode for a potassium-ion battery with unprecedented performance. *Angew. Chem. Int. Ed.* **2019**, 58, 10500-10505.
(67) Hu, X.; Jian, J.; Fang, Z.; Zhong, L.; Yuan, Z.; Yang, M.; Ren, S.; Zhang, Q.; Chen, X.; Yu, D. Hierarchical assemblies of conjugated ultrathin COF nanosheets for high-sulfur-loading and long-lifespan lithium-sulfur batteries: fully-exposed porphyrin matters. *Energy Storage Mater.* **2019**, 22, 40-47.
(68) Yang, Z.; Peng, C.; Meng, R.; Zu, L.; Feng, Y.; Chen, B.; Mi, Y.; Zhang, C.; Yang, J. Hybrid anatase/rutile nanodots-embedded covalent organic frameworks with complementary polysulfide adsorption for high-performance lithium-sulfur batteries. *ACS Cent. Sci.* **2019**, 5, 1876-1883.
(69) Meng, Y.; Lin, G.; Ding, H.; Liao, H.; Wang, C. Impregnation of sulfur into a 2D pyrene-based covalent organic framework for high-rate lithium-sulfur batteries. *J. Mater. Chem. A* **2018**, 6, 17186-17191.
(70) Duan, H.; Li, K.; Xie, M.; Chen, J. M.; Zhou, H. G.; Wu, X.; Ning, G. H.; Cooper, A. I.; Li, D. Scalable synthesis of ultrathin polyimide covalent organic framework nanosheets for high-performance lithium-sulfur batteries. *J. Am. Chem. Soc.* **2021**, 143, 19446-19453.
(71) Yusran, Y.; Li, H.; Guan, X.; Li, D.; Tang, L.; Xue, M.; Zhuang, Z.; Yan, Y.; Valtchev, V.; Qiu, S.; Fang, Q. Exfoliated mesoporous 2D covalent organic frameworks for high-rate electrochemical double-layer capacitors. *Adv. Mater.* **2020**, 32, e1907289.
(72) Lee, M. K.; Shokouhimehr, M.; Kim, S. Y.; Jang, H. W. Two- dimensional metal-organic frameworks and covalent-organic frameworks for electrocatalysis: distinct merits by the reduced dimension. *Adv. Energy Mater.* **2021**, 12, 2003990.
(73) Cui, X.; Gao, L.; Ma, R.; Wei, Z.; Lu, C.; Li, Z.; Yang, Y. Pyrolysis-free covalent organic framework-based materials for efficient oxygen electrocatalysis. *J. Mater. Chem. A* **2021**, 9, 20985-21004.
(74) Hu, T.; Wang, Y.; Xiao, H.; Chen, W.; Zhao, M.; Jia, J. Shape-control of super-branched Pd-Cu alloys with enhanced electrocatalytic performance for ethylene glycol oxidation. *Chem. Commun.* **2018**, 54, 13363-

DOI: 10.14102/j.cnki.0254-5861.2022-0114

13366.
(75) Yuan, D.; Dou, Y.; Wu, Z.; Tian, Y.; Ye, K. H.; Lin, Z.; Dou, S. X.; Zhang, S. Atomically thin materials for next-generation rechargeable batteries. *Chem. Rev.* **2022**, 122, 957-999.
(76) Cheng, Z.; Xie, M.; Mao, Y.; Ou, J.; Zhang, S.; Z.; Li, J.; Fu, F.; Wu, J.; Shen, Y.; Lu, D.; Chen, H. Building lithiophilic ion-conduction highways on garnet-type solid-state Li^+ conductors. *Adv. Energy Mater.* **2020**, 10, 1904230.
(77) Chen, D.; Huang, S.; Zhong, L.; Wang, S.; Xiao, M.; Han, D.; Meng, Y. In situ preparation of thin and rigid COF film on Li anode as artificial solid electrolyte interphase layer resisting li dendrite puncture. *Adv. Funct. Mater.* **2019**, 30, 1907717.
(78) Ren, Y.; Hortance, N.; McBride, J.; Hatzell, K. B. Sodium-sulfur batteries enabled by a protected inorganic/organic hybrid solid electrolyte. *ACS Energy Lett.* **2020**, 6, 345-353.
(79) Lau, J.; DeBlock, R. H.; Butts, D. M.; Ashby, D. S.; Choi, C. S.; Dunn, B. S. Sulfide solid electrolytes for lithium battery applications. *Adv. Energy Mater.* **2018**, 8, 1800933.
(80) Schwietert, T. K.; Arszelewska, V. A.; Wang, C.; Yu, C.; Vasileiadis, A.; De Klerk, N. J. J.; Hageman, J.; Hupfer, T.; Kerkamm, I.; Xu, Y.; Van der Maas, E.; Kelder, E. M.; Ganapathy, S.; Wagemaker, M. Clarifying the relationship between redox activity and electrochemical stability in solid electrolytes. *Nat. Mater.* **2020**, 19, 428-435.
(81) Zaman, W.; Hortance, N.; Dixit, M. B.; De Andrade, V.; Hatzell, K. B. Visualizing percolation and ion transport in hybrid solid electrolytes for Li-metal batteries. *J. Mater. Chem. A* **2019**, 7, 23914-23921.
(82) Xi, G.; Xiao, M.; Wang, S.; Han, D.; Li, Y.; Meng, Y. Polymer-based solid electrolytes: material selection, design, and application. *Adv. Funct. Mater.* **2020**, 31, 2007598.
(83) Pan, K.; Zhang, L.; Qian, W.; Wu, X.; Dong, K.; Zhang, H.; Zhang, S. A flexible ceramic/polymer hybrid solid electrolyte for solid-state lithium metal batteries. *Adv. Mater.* **2020**, 32, e2000399.
(84) Sen, S.; Trevisanello, E.; Niemöller, E.; Shi, B.; Simon, F. J.; Richter, F. H. The role of polymers in lithium solid-state batteries with inorganic solid electrolytes. *J. Mater. Chem. A* **2021**, 9, 18701-18732.
(85) Ye, T.; Li, L.; Zhang, Y. Recent progress in solid electrolytes for energy storage devices. *Adv. Funct. Mater.* **2020**, 30, 2000077.
(86) Lian, P.; Zhao, B.; Zhang, L.; Xu, N.; Wu, M.; Gao, X. Inorganic sulfide solid electrolytes for all-solid-state lithium secondary batteries. *J. Mater. Chem. A* **2019**, 7, 20540-20557.
(87) Vazquez-Molina, D. A.; Mohammad-Pour, G. S.; Lee, C.; Logan, M. W.; Duan, X.; Harper, J. K.; Uribe-Romo, F. J. Mechanically shaped two-dimensional covalent organic frameworks reveal crystallographic alignment and fast Li-ion conductivity. *J. Am. Chem. Soc.* **2016**, 138, 9767-9770.
(88) Xie, Z.; Wang, B.; Yang, Z.; Yang, X.; Yu, X.; Xing, G.; Zhang, Y.; Chen, L. Stable 2D heteroporous covalent organic frameworks for efficient ionic conduction. *Angew. Chem. Int. Ed.* **2019**, 58, 15742-15746.
(89) Guo, Z.; Zhang, Y.; Dong, Y.; Li, J.; Li, S.; Shao, P.; Feng, X.; Wang, B. Fast ion transport pathway provided by polyethylene glycol confined in covalent organic frameworks. *J. Am. Chem. Soc.* **2019**, 141, 1923-1927.
(90) Liu, Z.; Zhang, K.; Huang, G.; Bian, S.; Huang, Y.; Jiang, X.; Pan, Y.; Wang, Y.; Xia, X.; Xu, B.; Zhang, G. Lithium-ion transport in covalent organic framework membrane. *Chem. Eng. J.* **2022**, 433, 133550.
(91) Wang, S.; Li, X.; Cheng, T.; Liu, Y.; Li, Q.; Bai, M.; Liu, X.; Geng, H.; Lai, W.; Huang, W. Highly conjugated three-dimensional covalent organic frameworks with enhanced Li-ion conductivity as solid-state electrolytes for high-performance lithium metal batteries. *J. Mater. Chem. A* **2022**, 10, 8761-8771.
(92) Shan, Z.; Wu, M.; Du, Y.; Xu, B.; He, B.; Wu, X.; Zhang, G. Covalent organic framework-based electrolytes for fast Li^+ conduction and high-temperature solid-state lithium-ion batteries. *Chem. Mate.* **2021**, 33, 5058-5066.
(93) Xu, Q.; Tao, S.; Jiang, Q.; Jiang, D. Ion conduction in polyelectrolyte covalent organic frameworks. *J. Am. Chem. Soc.* **2018**, 140, 7429-7432.
(94) Zhang, G.; Hong, Y. L.; Nishiyama, Y.; Bai, S.; Kitagawa, S.; Horike, S. Accumulation of glassy poly(ethylene oxide) anchored in a covalent organic framework as a solid-state Li^+ electrolyte. *J. Am. Chem. Soc.* **2019**, 141, 1227-1234.
(95) Wang, Y.; Zhang, K.; Jiang, X.; Liu, Z.; Bian, S.; Pan, Y.; Shan, Z.; Wu, M.; Xu, B.; Zhang, G. Branched poly(ethylene glycol)-functionalized covalent organic frameworks as solid electrolytes. *ACS Appl. Energy Mater.* **2021**, 4, 11720-11725.
(96) Liu, Z.; Zhang, K.; Huang, G.; Xu, B.; Hong, Y. L.; Wu, X.; Nishiyama, Y.; Horike, S.; Zhang, G.; Kitagawa, S. Highly processable covalent organic framework gel electrolyte enabled by side-chain engineering for lithium-ion batteries. *Angew. Chem. Int. Ed.* **2022**, 61, e202110695.
(97) Xu, Q.; Tao, S.; Jiang, Q.; Jiang, D. Designing covalent organic frameworks with a tailored ionic interface for ion transport across one-dimensional channels. *Angew. Chem. Int. Ed.* **2020**, 59, 4557-4563.
(98) Du, Y.; Yang, H.; Whiteley, J. M.; Wan, S.; Jin, Y.; Lee, S. H.; Zhang, W. Ionic covalent organic frameworks with spiroborate linkage. *Angew. Chem. Int. Ed.* **2016**, 55, 1737-1741.
(99) Chen, H.; Tu, H.; Hu, C.; Liu, Y.; Dong, D.; Sun, Y.; Dai, Y.; Wang, S.; Qian, H.; Lin, Z.; Chen, L. Cationic covalent organic framework nanosheets for fast Li-ion conduction. *J. Am. Chem. Soc.* **2018**, 140, 896-899.
(100) Li, Z.; Liu, Z.; Mu, Z.; Cao, C.; Li, Z.; Wang, T.; Li, Y.; Ding, X.; Han, B.; Feng, W. Cationic covalent organic framework based all-solid-state electrolytes. *Mater. Chem. Front.* **2020**, 4, 1164-1173.
(101) Shaik, M. R.; Bissannagari, M.; Kwon, Y. M.; Cho, K. Y.; Kim, J.; Yoon, S. Soft, robust, Li-ion friendly halloysite-based hybrid protective layer for dendrite-free Li metal anode. *Chem. Eng. J.* **2021**, 424,
(102) Huang, L.; Xu, G.; Du, X.; Li, J.; Xie, B.; Liu, H.; Han, P.; Dong, S.; Cui, G.; Chen, L. Uncovering LiH triggered thermal runaway mechanism of a high-energy $LiNi_{0.5}Co_{0.2}Mn_{0.3}O_2$/graphite pouch cell. *Adv. Sci.* **2021**, 8, e2100676.
(103) Moyassari, E.; Streck, L.; Paul, N.; Trunk, M.; Neagu, R.; Chang, C.; Hou, S.; Märkisch, B.; Gilles, R.; Jossen, A. Impact of silicon content within silicon-graphite anodes on performance and li concentration profiles of Li-ion cells using neutron depth profiling. *J. Electrochem. Soc.* **2021**, 168, 020519.
(104) Guo, H.; Hou, G.; Li, D.; Sun, Q.; Ai, Q.; Si, P.; Min, G.; Lou, J.; Feng, J.; Ci, L. High current enabled stable lithium anode for ultralong cycling life of lithium-oxygen batteries. *ACS Appl. Mater. Inter.* **2019**, 11, 30793-30800.
(105) Jeong, K.; Park, S.; Jung, G. Y.; Kim, S. H.; Lee, Y. H.; Kwak, S. K.; Lee, S. Y. Solvent-free, single lithium-ion conducting covalent organic frameworks. *J. Am. Chem. Soc.* **2019**, 141, 5880-5885.
(106) Hu, Y.; Dunlap, N.; Wan, S.; Lu, S.; Huang, S.; Sellinger, I.; Ortiz, M.; Jin, Y.; Lee, S. H.; Zhang, W. Crystalline lithium imidazolate covalent organic frameworks with high Li-ion conductivity. *J. Am. Chem. Soc.* **2019**, 141, 7518-7525.

DOI: 10.14102/j.cnki.0254-5861.2022-0114

Chinese Journal of Structural Chemistry

(107) Meng, F.; Bi, S.; Sun, Z.; Jiang, B.; Wu, D.; Chen, J. S.; Zhang, F. Synthesis of ionic vinylene-linked covalent organic frameworks through quaternization-activated knoevenagel condensation. *Angew. Chem. Int. Ed.* **2021**, 60, 13614-13620.
(108) Guo, D.; Shinde, D. B.; Shin, W.; Abou-Hamad, E.; Emwas, A. H.; Lai, Z.; Manthiram, A. Foldable solid-state batteries enabled by electrolyte mediation in covalent organic frameworks. *Adv. Mater.* **2022**, e2201410.

Received: May 8, 2022
Accepted: May 17, 2022
Published online: May 23, 2022
Published: October 31, 2022

Sijia Liu received her BE degree in chemistry from Zhengzhou University in 2020. She is currently pursuing her MS degree in physical chemistry at the ShanghaiTech University, and under the supervision of Professor Qing Xu and Gaofeng Zeng at the Shanghai Advanced Research Institute, Chinese Academy of Sciences (CAS). Her current research focuses on the design and synthesis of COFs for electrocatalysis and batteries.

Minghao Liu was born in 1996. He received his master's degree in 2020 from University College London. He is a PhD student in environmental engineering under the supervision of Professor Gaofeng Zeng and Qing Xu at Shanghai Advanced Research Institute, Chinese Academy of Science (CAS). His current research interests involve the design and synthesis of COFs and metal organic frameworks (MOFs) for electrocatalysis and batteries.

Qing Xu received his MS degree in 2015 from Shanghai Jiao Tong University and PhD degree in 2018 from the Institute of Molecular Science (IMS), the Graduate University for Advanced Studies (SOKENDAI). He is an associate professor in Shanghai Advanced Research Institute, Chinese Academy of Sciences (CAS). His research interests focus on the synthesis and functionalization of porous polymers.

Prof. **Gaofeng Zeng** received his BS in Chemical Engineering from Dalian University of Technology (DUT) and PhD in Industrial Catalysis from Dalian Institute of Chemical Physics, Chinese Academy of Sciences (DICP). Prior to Shanghai Advanced Research Institute, Chinese Academy of Sciences (SARI), he worked as a post-doc fellow at King Abdullah University of Science and Technology (KAUST) for three years. Currently, he is a professor and group leader at SARI and his research activities cover the synthesis of advanced porous/membrane materials and the corresponding applications in separations and reactions. He has >80 refereed journal articles and > 30 patents.

DOI: 10.14102/j.cnki.0254-5861.2022-0114